Development of a genetically-encoded sensor for probing endogenous nociceptin opioid peptide release

Xuehan Zhou[1,2,#], Carrie Stine[3,4,5,#], Patricia Oliveira Prada[6,7,8], Debora Fusca[7,9], Kevin Assoumou[10], Jan Dernic[1], Musadiq A. Bhat[1], Ananya S. Achanta[3,4], Joseph C. Johnson[3,4], Sanjana Jadhav[3,4], Corinna A. Bader[6,7], Lukas Steuernagel[6,7], Luca Ravotto[1], Dietmar Benke[1,2], Bruno Weber[1,2], Miriam Stoeber[10], Peter Kloppenburg[7,9], Jens C. Brüning[6,7,11], Michael R. Bruchas[3,4,5,*], Tommaso Patriarchi[1,2,*]

[1] Institute of Pharmacology and Toxicology, University of Zürich, Zürich, Switzerland;

[2] Neuroscience Center Zurich, University and ETH Zürich, Zürich, Switzerland;

[3] Center for the Neurobiology of Addiction, Pain, and Emotion, University of Washington, Seattle, USA;

[4] Departments of Anesthesiology and Pharmacology and Bioengineering, University of Washington, Seattle, USA;

[5] Molecular and Cellular Biology, University of Washington School of Medicine, Seattle, USA;

[6] Max Planck Institute for Metabolism Research, Cologne, Germany;

[7] Excellence Cluster on Cellular Stress Responses in Aging Associated Diseases (CECAD) and Center for Molecular Medicine Cologne (CMMC), University of Cologne, Germany

[8] School of Applied Sciences, State University of Campinas (UNICAMP), Limeira, Sao Paulo, Brazil;

[9] Institute of Zoology, Department of Biology, University of Cologne, Germany

[10] Department of Cell Physiology and Metabolism, University of Geneva, Geneva, Switzerland;

[11] Policlinic for Endocrinology, Diabetes and Preventive Medicine (PEDP), University Hospital Cologne, Germany.

[#] These authors contributed equally

[*]correspondence should be addressed to: patriarchi@pharma.uzh.ch or mbruchas@uw.edu

Abstract

Nociceptin/orphanin-FQ (N/OFQ) is a recently appreciated critical opioid peptide with key regulatory functions in several central behavioral processes including motivation, stress, feeding, and sleep. The functional relevance of N/OFQ action in the mammalian brain remains unclear due to a lack of high-resolution approaches to detect this neuropeptide with appropriate spatial and temporal resolution. Here we develop and characterize NOPLight, a genetically encoded sensor that sensitively reports changes in endogenous N/OFQ release. We characterized the affinity, pharmacological profile, spectral properties, kinetics, ligand selectivity, and potential interaction with intracellular signal transducers of NOPLight in vitro. Its functionality was established in acute brain slices by exogeneous N/OFQ application and chemogenetic induction of endogenous N/OFQ release from PNOC neurons. In vivo studies with fiber photometry enabled a direct recording of binding by N/OFQ receptor ligands, as well as the detection of natural or chemogenetically-evoked endogenous N/OFQ release within the paranigral ventral tegmental area (pnVTA). In summary, we show that NOPLight can be used to detect N/OFQ opioid peptide signal dynamics in tissue and freely-behaving animals.

Introduction

The nociceptin/orphanin-FQ peptide (N/OFQ) along with its cognate receptor (NOPR) represent the most recently-discovered opioid peptide/receptor system[1,2]. NOPR is a G protein-coupled receptor (GPCR) and shares 60% of sequence similarity with the other members in the opioid family[3], while retaining a unique pharmacological profile[4]. Upon occupancy by N/OFQ, NOPR's endogenous peptide ligand, the receptor activates downstream Gi/Go proteins and induces intracellular signaling that includes the inhibition of cAMP formation and ultimately reduces neurotransmission via inhibition of voltage-gated calcium channels, and the activation of inwardly-rectifying potassium channels[5].

NOPR is abundantly expressed within the central nervous system[6–8], in line with the broad range of neural and cognitive functions regulated by this endogenous opioid system[9,10]. In particular, NOPR and preproN/OFQ (PNOC)-expressing neurons are highly enriched in the ventral tegmental area (VTA), arcuate nucleus of the hypothalamus (ARC), dorsal striatum, nucleus accumbens (NAc) and medial prefrontal cortex (mPFC)[7]. Being the major source of dopamine to limbic and forebrain regions, the VTA plays an important part in neural circuits regulating motivation and reward-based learning[11,12]. It is well established that VTA dopaminergic projections to the NAc are essential for encoding reward prediction and adaptive motivated behaviour towards both beneficial and aversive stimuli[13]. Several studies have shown that the N/OFQ system exerts an important modulatory effect on mesolimbic dopaminergic circuits. For example, intracerebroventricular (ICV) injection of N/OFQ produces a decrease in extracellular dopamine in the NAc[14] and exerts an inhibitory constraint on dopamine transmission by either inhibiting tyrosine hydroxylase phosphorylation or dopamine D1 receptor signalling[15]. At behavioural level, N/OFQ has been shown to prevent morphine- and cocaine-induced dopamine increase in the NAc[16,17], and inhibits conditioned place preference to morphine, amphetamine and cocaine[18,19], while disruption of the N/OFQ system is associated with motivated responding disorder[20]. ICV administration of N/OFQ was reported to potently block reward-associated cues but showed no effect on aversion associated cues[21].

In a recent study we identified a subgroup of PNOC-enriched neurons located in the paranigral VTA which, when activated, caused avoidance and decreased motivation for reward[22].

A separate population of PNOC neurons located in the ARC has emerged as an important neuronal population involved in regulating feeding behavior. These GABA-expressing neurons are activated after three days of a high-palatable, energy-dense diet and have been found to play a crucial role in feeding control. In particular, optogenetic stimulation of PNOC-expressing neurons in the ARC induces feeding, while selective ablation of these neurons decreases food intake and prevents obesity[23]. Apart from its roles in the VTA-NAc and ARC circuits, N/OFQ can inhibit mPFC-projecting VTA neurons[24] and a reduction in mPFC N/OFQ level was reported in rodents that underwent conditioned opioid withdrawal[25].

Of note, past studies on N/OFQ signalling have generated some contradictory results[26]. Activation of the NOPR with a selective agonist was reported to reduce alcohol drinking and seeking behavior[27,28], but a selective NOPR antagonist, LY2940094, was reported to have the same effect[29]. In anxiety-related behaviours, it has been reported that central injection of a NOPR agonist induces an anxiogenic effect, but anxiolytic effects of NOPR agonists are also reported[30–32]. These observations can be interpreted in different ways. The dynamics of NOPR desensitization after application of agonists or antagonists, for example, could contribute to the contradictory results. Another possible explanation could be the competition of different local neural circuits simultaneously recruited by the N/OFQ system, as most of the studies mentioned before do not have fine spatial control over the application of drugs nor the resolution to isolate endogenous release dynamics of the peptide. Overall, the exact mechanism of the NOPR-N/OFQ system and its impact on different neural circuits are, at best, only partially understood.

A major factor hindering a clear understanding of N/OFQ regulation of neural circuits, or any neuropeptide signalling system, are the major limitations imposed by current tools and

techniques used to detect the release of neuropeptides in living systems. Conventional techniques such as microdialysis and mass spectrometry-coupled high-performance liquid chromatography can successfully detect picomolar level of neuropeptides in extracellular fluid[33], yet the spatial and temporal resolution of these techniques is limited to single point measurements and long timescales on the order of several minutes[34]. This resolution is far from ideal for decoding the neuronal mechanisms of dynamic peptide action in vivo. New approaches to probing the nervous system using fluorescent sensors have started to gain traction across the field[35–39]. Combined with rapidly developing fluorescent recording and imaging techniques, these sensor-based approaches are uniquely suited in vivo observations with fine spatiotemporal resolution than was previously possible[35,40,41].

Here we report the development of NOPLight, a novel genetically-encoded opioid peptide sensor that provides a specific and sensitive fluorescence readout of endogenous N/OFQ dynamics with unprecedented temporal resolution ex vivo and in vivo. Using the sensor we could detect ligand binding by systemically administered NOPR agonists and antagonists in the central nervous system. We also probed both chemogenetically-evoked and behaviorally-induced dynamics of endogenous N/OFQ in freely moving mice. Thus, NOPLight extends the neuropeptide molecular toolbox necessary to investigate the physiology of neuropeptides and in particular this important endogenous opioid system with high resolution.

Results

Development of a genetically-encoded N/OFQ opioid peptide (N/OFQ) sensor

To develop a fluorescent sensor for N/OFQ, we started by designing a prototype sensor based on the human NOPR which has 93-94% sequence homology to the mouse and rat receptors. We replaced the third intracellular loop (ICL3) with a cpGFP module that was previously optimized during the development of the dLight1 family of dopamine sensors[42] (**Fig. 1a,**

Supplementary Fig. 1a). This initial construct exhibited poor membrane expression and no fluorescent response to N/OFQ (**Supplementary Fig. 1b**). Given the pivotal role of the GPCR C-terminus in trafficking[43], we reasoned that replacement of the NOPR C-terminus with that of another opioid receptor may facilitate membrane targeting of the sensor. Based on our prior experience[42], we chose to use the C-terminus from the kappa-type opioid receptor. The resulting chimeric receptor showed improved expression at the cell surface, but still exhibited a small response to N/OFQ (**Supplementary Fig. 1b**). We then aimed to improve the dynamic range of the sensor through mutagenesis efforts. First, we elongated the N-terminal cpGFP linker with additional amino acids originating from dLight1[42]. This led to the identification of a variant with a fluorescent response ($\Delta F/F_0$) of approximately 100% (**Supplementary Fig. 1c-d**). As a next step, we performed targeted mutagenesis efforts focused on the second intracellular loop (ICL2) of the sensor. Through these efforts we identified a beneficial mutation ($I156^{34.51}K$, **Supplementary Fig. 1e**) that was then carried forward onto the next rounds of screening focused on receptor and cpGFP residues around the insertion site of the fluorescent protein between transmembrane helixes 5/6 (TM5/TM6) (**Supplementary Fig. 1e**). The final variant, which was named NOPLight, had a $\Delta F/F_0$ of 388% in transfected HEK293T cells and a similar performance in transduced neuron culture ($\Delta F/F_0$ = 378%) upon activation by the high affinity, full agonist N/OFQ (**Fig. 1b**). Furthermore, the evoked fluorescence signal could be reversed to baseline levels using the selective and competitive small molecule antagonist J-113397 (**Fig. 1c**). To aid the subsequent characterization experiments we also developed a control sensor, NOPLight-Ctr, by mutating into alanine two key residues (D110, D130) located in the binding pocket of NOPR[4] (**Supplementary Fig. 2a**). The control sensor was well expressed on the surface of HEK293T cells and neurons but showed no response to N/OFQ (**Fig. 1c-d, Supplementary Fig. 2a**), or to a panel of other endogenous opioids or fast neurotransmitters, including dopamine, acetylcholine and GABA. (**Supplementary Fig. 2b**).

In vitro characterization of NOPLight

To better examine the properties of the sensor, we first characterized the apparent ligand affinity of NOPLight in vitro, using NOPLight-expressing HEK293T cells and cultured neurons. In HEK293T cells the endogenous ligand N/OFQ elicited a fluorescent response of NOPLight at a half maximal effective concentration (EC_{50}) of 28.65 ± 5.1 nM, whereas in cultured neurons it showed an EC_{50} of 42.81 ± 5.4 nM (**Fig. 1e**), approximately one order of magnitude lower than the reported potency of N/OFQ to the wild type NOPR in the central nervous system[44]. To determine the activation kinetics of NOPLight, we measured the activation of NOPLight upon direct bath-application of N/OFQ using high-speed line-scan confocal imaging. Mono-exponential fitting of the NOPLight fluorescence response indicated a subsecond time constant of signal activation at the sensor (τ_{ON} = 595 ± 69 ms; **Fig. 1f**).

Next, we characterized the pharmacological profile of NOPLight. We tested the response of NOPLight-expressing HEK293T cells to a panel of small-molecule and peptide ligands that are known to be NOPR agonists or antagonists. Of the antagonist compounds tested only nocistatin had a very small effect on the signal induced by N/OFQ. On the contrary, the antagonist peptide UFP-101 and the small molecule compound J-113397 produced robust competitive antagonism, fully reversing the activation of NOPLight at the concentrations used (1 μM). Importantly, none of the antagonists ligands elicited a response when applied alone to sensor-expressing cells. On the other hand, we could clearly detect positive fluorescence responses of NOPLight to several types of selective NOPR agonist compounds. In particular the full agonist Ro-64 elicited the largest fluorescent response in this assay ($\Delta F/F_0$ = 323%) and produced a response of similarly large magnitude in NOPLight-expressing primary neuronal cultures ($\Delta F/F_0$ = 221%) (**Supplementary Fig. 2c-f**). Interestingly, all of the agonist compounds tested induced an overall smaller fluorescence response than N/OFQ itself, indicative of partial agonism at NOPLight (**Fig. 1g**).

We then characterized the spectral properties of NOPLight. Under both one-photon and two-photon illumination, NOPLight exhibited similar spectral characteristics as other GPCR-based sensors[42,45]. The sensor had an isosbestic point at around 440 nm and peak performance at 472 nm and 920/990 nm, respectively (**Supplementary Fig. 3a-b**). The parent receptor of

NOPLight, NOPR, is known to respond with a uniquely high degree of selectivity to N/OFQ, as compared to all other endogenous opioid peptides[3,46]. To ensure that the NOPLight retained the same degree of ligand-selectivity, we tested its response to a series of opioids peptides applied to NOPLight-expressing cells at a high concentration (1 μM). NOPLight showed no response to dynorphins, enkephalins and β-endorphin (**Fig. 1h**). Similarly, the sensor did not respond to a panel of fast neurotransmitters (**Fig. 1i**), indicating high N/OFQ ligand selectivity at NOPLight.

To ensure minimal interference of NOPLight with cellular physiology, we investigated the putative coupling of the sensor with downstream intracellular signalling pathways and compared it to that of wild-type human NOPR. Like the other members of the opioid receptor family, NOPR is Gi/o coupled and inhibits basal and Gs-stimulated adenylate cyclase activity upon activation, thus lowering intracellular cAMP levels[3,46]. We used the GloSensor cAMP assay in HEK293 cells expressing either wild-type human NOPR or NOPLight to monitor cAMP production with a bioluminescence readout. Application of 1 nM N/OFQ significantly inhibited the forskolin-induced cAMP response in cells expressing the NOPR, while no effect was observed for NOPLight-expressing cells treated with up to 100 nM N/OFQ (**Supplementary Fig. 4a**). At higher concentrations of N/OFQ, inhibition of the cAMP signal in NOPLight-expressing cells was still significantly reduced compared to that of NOPR. Under physiological conditions, activation of GPCRs can induce β-arrestin recruitment and/or receptor internalization. We monitored β-arrestin-2 recruitment to the cell surface upon N/OFQ stimulation using TIRF microscopy. Activation of NOPR induced strong β-arrestin-2 recruitment and subsequent internalization of the receptor, whereas NOPLight showed neither of these effects after prolonged occupancy by N/OFQ (**Supplementary Fig. 4b-e**). In accordance with the lack of coupling to β-arrestin-2, we also observed that the NOPLight response remained stable for over 1.5 hours in the presence of N/OFQ, and the increase in fluorescence could be reversed by treating the cells with a membrane-impermeable peptide NOPR antagonist (UFP-101, 100 nM; **Supplementary Fig. 4f-g**). These results indicate that while NOPLight retains the ligand selectivity of its parent receptor, its cellular expression has

a very low likelihood of interfering with intracellular signaling; thus the sensor can be meaningfully utilized in physiological settings.

Ex vivo characterization of NOPLight

We then expressed the sensor directly in brain tissue by injecting NOPLight-encoding adeno-associated virus (AAVDJ-hSyn-NOPLight) in the arcuate nucleus (ARC) of the hypothalamus of wild-type mice. After 4 weeks of expression, the sensor was clearly expressed and was characterized for its functional response to exogenously perfused N/OFQ (**Fig. 2a-b**). NOPLight responses could be detected from ROIs in the ARC upon superfusion of as little as 10 nM N/OFQ on the slice ($\Delta F/F_0$ = 1.9 ± 1.1%, n = 10), and the magnitude of the responses kept increasing up to the highest N/OFQ concentration tested (10 µM, $\Delta F/F_0$ = 73 ± 21%) (**Fig. 2c**). We next tested whether the *in situ* sensitivity of NOPLight would be sufficient to detect endogenous N/OFQ release in this ex vivo setting. For this purpose, we again used the preparation of ARC neurons with NOPLight expression and additionally expressed the activating DREADD hM3D in PNOC neurons (**Fig. 2d, e**). For this, a hM3Dq-encoding adeno-associated virus (AAV8-hSyn-DIO-hM3Dq-mcherry) was injected into the ARC of PNOC-Cre mice, enabling Cre-dependent expression of hM3Dq. hM3Dq activation by bath-applied clozapine N-oxide (CNO) evoked a clear increase in the firing rate of PNOC neurons that lasted for several minutes (**Fig. 2f**). Correspondingly, we could detect an increase in NOPLight responses with a mean fluorescence change of $\Delta F/F_0$ = 1.6 ± 0.3% (**Figure 2g-i**), indicating that the sensor could report endogenous N/OFQ release under these conditions. The response of NOPLight was reversible and reflected the time course of chemogenetic activation of PNOC neurons. Overall, these results indicate that NOPLight provides a sensitive and specific readout of both superfused as well as endogenous N/OFQ peptide release in brain tissue.

NOPLight activation by an exogenous NOPR agonist *in vivo*

Our in vitro results (**Fig. 1g**) showed potent and efficacious NOPLight responses to the small molecule NOPR agonist Ro-64. Thus, we next determined whether we could use in vivo fiber photometry to record NOPLight fluorescence in vivo to track target engagement of this NOPR agonist action in real-time within the brain (**Fig 3**). To do so, we injected WT mice with AAV-DJ-hSyn-NOPLight either in the VTA or in the ARC and implanted optic fibers above the injection sites for photometry recordings (**Fig. 3a-b, Supplementary Fig. 5**). At 3-4 weeks post-viral injection, we detected robust, dose-dependent increases in NOPLight fluorescence in both brain areas following systemic (i.p.) injection of increasing doses of Ro-64 (**Fig. 3c**, **Supplementary Fig. 5a-d**). To determine if the observed increase in NOPLight fluorescence was produced by the sensor's detection of the NOPR agonist, we pretreated animals with two different selective NOPR antagonists, LY2940094 (LY, 10 mg/kg o.g.) or J-113397 (J11, 10 mg/kg i.p.) 30 minutes prior to injection of Ro-64. Both NOPR-selective antagonists fully inhibited the agonist-induced fluorescent signal (**Fig. 3d-e**). Upon closer inspection of the raw unprocessed signal and isosbestic photometry recordings, we discovered that the 405 nm wavelength, which is commonly used as the isosbestic point for green-fluorescing sensors[47,48], had a small but notable increase in the presence of the NOPR agonist (**Supplementary Fig. 6**). This unexpected result suggests that 405 nm is not the most suitable isosbestic point for NOPLight, in line with our spectral characterization of the sensor (**Supplementary Fig. 3a-b**). Next, we injected additional cohorts of PNOC-Cre or WT mice in the VTA with AAVs containing either a Cre-dependent variant of NOPLight (AAV-DJ-hSyn-FLEX-NOPLight), or the control sensor (AAV-DJ-hSyn-NOPLight.ctr) respectively, with optical fibers implanted above the injection site (**Fig. 3f**). We found that systemic injection of 10 mg/kg Ro-64 produces a robust increase in Flex NOPLight signal that is not significantly different from the agonist-induced signal we recorded from non-conditionally expressed NOPLight (**Fig. 3g-h**). In contrast, the control sensor showed no fluorescent response with 10 mg/kg Ro-64 injection (**Fig. 3g-h**). These results indicate that NOPLight expressed in freely moving animals reliably provides dose-dependent and antagonist-sensitive detection of exogenous NOPR agonists in real time.

NOPLight detection of evoked endogenous N/OFQ release *in vivo*

A primary goal motivating our development of the NOPLight sensor is to ultimately achieve real-time detection of local N/OFQ release in behaving animals. Thus, our next step toward this goal was to determine whether NOPLight reliably detects endogenously released N/OFQ. To accomplish this, we evoked endogenous N/OFQ release in a local paranigral VTA (pnVTA) circuit we previously identified[22] by using a chemogenetic approach to selectively activate VTA^{PNOC} neurons while simultaneously recording changes in VTA-NOPLight fluorescence via fiber photometry. PNOC-Cre mice were co-injected in the VTA with two Cre-dependent AAVs containing i) AAV-DH-hSyn-NOPLight and ii) an mScarlet-tagged stimulatory hM3Dq DREADD (AAV5-EF1a-DIO-HA-hM3D(Gq)-mScarlet), with optical fibers implanted above the injection site (**Fig. 4a**). Control animals received an mCherry (AAV5-EF1a-DIO-mCherry) injection in place of the red fluorophore-tagged DREADD. Based on our earlier observations that 405 nm may not be the appropriate isosbestic point for NOPLight (**Supplementary Figs. 3 and 6**), we tested and characterized an alternative set of LED wavelengths in this group of experiments, using 435 nm and 490 nm as the isosbestic and signal wavelengths, respectively. Activation of the hM3Dq DREADD via systemic injection with 5 mg/kg of clozapine-N-oxide (CNO) produced a significant increase in NOPLight fluorescence that was not observed in the control animals that had mCherry expression in place of the DREADD (**Fig. 4b**). We next sought confirmation that this increase was truly the result of chemogenetically-evoked endogenous N/OFQ release, and thus acting via a NOPR-dependent mechanism. Pre-treatment with the selective NOPR antagonist LY2940094[49] 30 minutes prior to CNO injection prevented the CNO-induced increase in NOPLight fluorescence (**Fig. 4c**). Together, these results provide strong evidence that NOPLight can detect evoked endogenous release of N/OFQ in freely moving animals.

Monitoring endogenous N/OFQ dynamics in reward-related operant behavior

We next examined NOPLight's ability to report transient, endogenous N/OFQ release evoked by different naturalistic behavioral states. N/OFQ and its receptor NOPR have been implicated in neuromodulation of a wide variety of essential behavioral processes including stress, aversion, motivation, reward seeking, and feeding[22,23,27,50–55]. We previously identified a role for VTA N/OFQ signaling in reward-related and aversive behavior, and extensively characterized the calcium activity of pnVTA^{PNOC} neurons during operant responding for reward. Therefore, we injected WT mice with AAV-DJ-hSyn-NOPLight in the VTA and implanted optical fibers above the injection site to allow for fiber photometry recordings of NOPLight during operant conditioning (**Fig. 5a**). Food-restricted mice (to ~85-90% of their bodyweight) first underwent Pavlovian conditioning to associate a 5-second house light cue (CS) with delivery of a sucrose pellet (US). Next, mice were trained on a fixed ratio (FR) operant schedule, learning first to perform one (FR1) and later three (FR3) nose pokes into an active port in order to receive the light cue and sucrose reward. Finally, mice were placed in a progressive ratio (PR) test, where the required nose poke criterion increases exponentially with each subsequent reward until the mice reach a motivational breakpoint where they are unwilling to exert any further effort to obtain a reward (**Fig. 5b**). Tracking of pellet consumption across the training paradigm confirmed that mice were consuming the vast majority of rewards they obtained, and thus it is likely they were not making active nose pokes simply as a compulsive response (**Fig. 5c**). Mice also successfully learned that only the active port would result in reward delivery, consistently making the majority of their nose pokes into the active port (**Fig. 5d**).

NOPLight fluorescent signals recorded during early Pavlovian conditioning showed a sharp increase in response to onset of the light cue (**Fig. 5e**), consistent with fiber photometry recordings of the calcium activity (GCaMP6s) of a posterior population of pnVTA^{PNOC} neurons known to project locally within the VTA[22]. Across all Pavlovian and operant conditioning schedules, we observed a robust decrease in NOPLight fluorescence persistent throughout the reward consumption period that was immediately followed by a transient increase in signal upon the end of a feeding bout (**Fig. 5e-h**). This decrease in signal during reward consumption

and subsequent increase at the end of the feeding period is consistent with previously reported calcium activity patterns of posterior pnVTA^{PNOC} neurons recorded during both Pavlovian and operant conditioning. Importantly, during FR3 and PR recordings when mice performed an active nose poke that did not yet meet the threshold for a reward delivery we did not observe a decrease in NOPLight fluorescence following the nose poke, indicating that the decrease is related to reward consumption and not the operant action (**Fig. 5g-h**). Taken together, the NOPLight fluorescent signal closely resembles known patterns of pnVTA^{PNOC} neuron GCaMP activity during reward-seeking and consumption behaviors. These results indicate that NOPLight is useful for detecting endogenous N/OFQ release during behavioral epochs.

Our earlier results indicated that 435 nm is an isosbestic point for NOPLight (**Supplementary Figs. 3 and 6**). We did not use a 405-channel subtraction in analysis of the operant conditioning signal, creating the possibility that the fluorescent changes we recorded could be attributed to motion artefact. To address this possibility, several weeks after the PR test we re-tested the animals in a single FR1 session recording with 435 nm and 490 nm LEDs as the isosbestic and signal wavelengths, respectively. Since the largest changes in NOPLight signal we observed in FR1 were primarily during reward consumption, we compared the new motion-corrected signal with the 470 nm signal from an earlier FR1 session during trials where animals consumed the reward. Aligning these traces revealed similar overall trends, with an increase during the cue period followed by a dip and then subsequent increase in fluorescence, presumably upon the end of pellet consumption (**Supplementary Fig. 7c**). The timing of the dip and subsequent increase were not entirely consistent however between the two traces, which may have been the result of a greater delay to pellet retrieval during some trials of the more recent session. To address this, we aligned the signal to the start of each pellet consumption bout which resulted in a much tighter similarity between both the trend and timing of the two traces (**Supplementary Fig. 7d**). These results suggest that the initially recorded signal without motion-correction likely does reflect true NOPLight signal.

Monitoring endogenous N/OFQ dynamics in response to aversive stimuli

To further characterize NOPLight's utility in detecting naturalistic N/OFQ dynamics, we also evaluated NOPLight fluorescence during aversive behavior. WT mice expressing AAV-DJ-hSyn-NOPLight in the VTA were implanted with optical fibers and head rings to allow for simultaneous fiber photometry recording and head-fixation[56], respectively. Mice were head-fixed during the recording session to reduce motion artefacts and received a 2-second-long toe pinch four times over one session, with each pinch separated by a 2-minute intertrial interval. This paradigm was repeated in a counterbalanced manner using either 405 nm and 470 nm or 435 nm and 490 nm LEDs to thoroughly characterize the response of this sensor upon excitation at different control wavelengths in vivo. The acute toe pinch produced a brief increase in NOPLight fluorescence rapidly followed by a robust decrease in the signal (**Supplementary Fig. 8a,c**). The signal recorded from the 470 nm and 490 nm LEDs was identical, suggesting equivalent rationale for using either wavelength for sensor photo-excitation. Notably, the 405 nm trace closely resembled the 470nm trace throughout the session, while the 435 nm remained more stable with only minor fluctuations (**Supplementary Fig. 8b,d**). Taken together, these recordings demonstrate NOPLight's ability to detect behaviorally-induced dynamic changes in endogenous N/OFQ in response to aversive stimuli, while also further supporting evidence that 435 nm is a more appropriate isosbestic point than 405 nm for in vivo use.

Discussion

Here we describe the engineering, characterization, and application of a novel genetically-encoded sensor (NOPLight) for monitoring the opioid neuropeptide N/OFQ in vitro, ex vivo, and in vivo. Endogenous opioid peptides represent one of the largest classes of neuropeptide families, yet detecting their release, dynamics, and properties in vitro and in vivo has been a challenge for over 60 years since their discovery[57–59]. We sought to develop a sensor which could detect: 1) evoked release, 2) endogenous release during naturalistic behavior, and 3) exogenous ligands in vivo to inform brain localization of pharmacological agents. These properties have been long sought after to better understand neuropeptide transmission generally, and more specifically opioid peptides and their actions.

The neuropeptide biosensor we developed here exhibits a large dynamic range both in HEK293T cells and in neurons, sub-second activation kinetics, very high ligand selectivity, a similar pharmacological profile to that of NOPR, and no detectable interference with endogenous signaling pathways. We demonstrated that NOPLight dose-dependently responds to systemic administration of a NOPR agonist, with sensitivity to blockade by selective NOPR antagonists. NOPLight is also capable of detecting endogenous release of N/OFQ evoked by either chemogenetic stimulation (hM3Dq DREADD) of PNOC neurons or during natural behavior.

Previous calcium activity recordings of PNOC neurons with local input in the VTA during operant conditioning tasks revealed dynamic engagement of $pnVTA^{PNOC}$ neurons during reward-seeking and consumption behavior[22]. While in many cases calcium mobilization is required for dense core vesicle fusion[60], calcium activity is not a direct correlate for peptide release and as such the dynamics of released N/OFQ could not be established in this prior study. Here we report NOPLight activity in the VTA in reward-seeking behavior during fixed ratio-1, -3, and progressive ratio paradigms, which identified a ramping increase in N/OFQ leading up to the act of performing the operant action (an active port nose poke), a rapid and sustained decrease during reward consumption, and a transient increase after consumption had ended (**Fig. 5**). This pattern of NOPLight signal closely resembles the expected dynamics

of N/OFQ release based on the prior study's calcium activity recordings[22]. Notably, we observed both dynamic increases and decreases in NOPLight fluorescence during behavioral epochs, suggesting that the NOPLight can be used to detect changes in peptide tone over behaviorally-relevant timescales. These data also provide the ability to align neuronal activity measured either by calcium dynamics or electrophysiology with neuropeptide release during freely-moving behaviorial epochs. Given the recent discoveries that PNOC and NOPR are important for motivation, feeding, and sleep induction[22,23,50–53], understanding the dynamic properties of this opioid peptide system is now of even greater importance as this receptor is now considered a major target for insomnia, addiction, and depression[49,61,62].

The endogenous activity of PNOC neurons in the VTA is thought to provide inhibitory tone onto VTA dopamine neurons, constraining motivation to seek rewards[15,22,24,63–65]. Here we observed an increase in NOPLight fluorescence upon the end of reward consumption. Since NOPR is largely expressed on dopamine neurons in the VTA and exerts inhibitory influence over their activity[24,63], it is possible that this increase in endogenous N/OFQ release after consumption reflects a temporarily satiated state where N/OFQ signaling transiently increases to suppress tonic dopamine neuron activity, thus reducing motivation to seek out additional rewards. Importantly, this is the first detection of real-time N/OFQ release in this context. As a result, these findings provide insight into the dynamics of N/OFQ signaling in the VTA which acts to coordinate motivated behavior through dopaminergic interactions.

We tested the performance of the sensor in vivo using different wavelength pairs. Following the development of GCaMPs, sensor excitation has conventionally employed a 405 nm wavelength light as a read-out for non-ligand sensitive signals (known as the isosbestic channel), that typically acts as an internal control for fiber photometry experiments, particularly in freely moving animals[47,48]. As a result, most commercially-available photometry setups are tailored to accommodate this wavelength. In this work we noted that, based on the results from our spectral characterization of NOPLight, excitation at a wavelength of 435 nm is better suited as a control 'isosbestic' channel. It is particularly worth noting that many recently-developed intensiometric GPCR-based biosensors exhibit a similar spectral property with a

right-shifted isosbestic point (i.e. > 420 nm)[45,66–69]. In these cases, use of 405 nm as the isosbestic channel for these sensors may lead to confounding results, difficulty in interpretation, and misguided conclusions.

Since it may be cost and time prohibitive for research groups to add an alternative recording parameter to existing photometry setups, we also demonstrate here that NOPLight signal recorded without an isosbestic-based motion correction can still detect the same trends in endogenous N/OFQ release as a 435 nm corrected recording. It is noteworthy that this will depend on the behavioral assay and photometry setup. In addition, head-fixation and red fluorophore-based motion controls are commonly used as alternatives to isosbestic controls that could easily be implemented with NOPLight[48,70]. Our careful evaluation and side-by-side comparison of different isosbestic and excitation wavelengths provide valuable insight into its photophysical properties that will help inform successful application of NOPLight and other neuropeptide sensors in future studies.

Our findings present NOPLight as a unique approach to improve investigations of endogenous opioid peptide dynamics with unparalleled spatiotemporal resolution. We characterized NOPLight expression, selectivity, and sensitivity to endogenous N/OFQ release both in vivo and in vitro. Future optimization of the sensor should seek to improve quantum yield (fluorescent readout) at lower peptide concentrations and to develop red-shifted variants to provide more flexibility in multiplexing NOPLight with other optical tools and sensors. This sensor directly helps to address a longstanding limitation in understanding the real-time dynamics of endogenous peptide release during behavioral epochs. Future applications of neuropeptide sensors such as NOPLight will advance our understanding of the underlying mechanisms by which endogenous opioid peptides control, stabilize and modulate neural circuits to regulate behavior.

Methods

Molecular cloning and structural modelling

The prototype sensor was designed *in silico* by sequence alignment (Clustal Omega2) and ordered as a geneblock (Thermo Fisher) flanked by HindIII and NotI restriction sites to be subsequently cloned into pCMV vector (Addgene #111053). For sensor optimization, site directed mutagenesis and Circular Polymerase Extension Cloning was performed by polymerase chain reaction with custom designed primers using a Pfu-Ultra II fusion High Fidelity DNA Polymerase (Agilent). Sanger sequencing (Microsynth) was performed for all constructs reported in the manuscript. The structural prediction of the NOPLight was generated by a deep learning-based modelling method, RoseTTAFold[4].

Cell culture, confocal imaging and quantification

HEK293T cells (ATCC CRL-3216) were authenticated by the vendor. They were seeded in glass bottom 35mm (MatTek, P35G-1.4-14-C) or 24-well plates (Cellvis, P24-0-N) and cultured in Dulbecco's modified Eagle's medium (Gibco) with 10% Fetal Bovine Serum (Gibco) and antibiotic-antimycotic (1:100 from 10,000 units/ml penicillin; 10,000 µg/ml streptomycin, 25 µg/ml amphotericin B, Gibco) mix at 37°C and 5% CO2. Cells were transduced at 70% confluency using Effectene transfection kit (QIAGEN) and imaged after 24 – 48 hours. Primary neuronal cultures were prepared as the following: the cerebral cortex of 18 days old rat embryos was carefully dissected and washed with 5 ml sterile-filtered PBGA buffer (PBS containing 10 mM glucose, 1 mg/ml bovine serum albumin and antibiotic-antimycotic 1:100 (10,000 units/ml penicillin; 10,000 µg/ml streptomycin; 25 µg/ml amphotericin B)). The cortices were cut into small pieces with a sterile scalpel and digested in 5 ml sterile filtered papain solution for 15 min at 37°C. The supernatant was removed, and tissue washed twice with complete DMEM/FCS medium (Dulbecco's Modified Eagle's Medium containing 10% Fetal Calf Serum and penicillin/streptomycin, 1:100). Fresh DMEM/FCS was then added, and the tissue gently triturated and subsequently filtered through a 40 µm cell-strainer. Finally, the

neurons were plated at a concentration of 40,000-50,000 cells per well onto the poly-L-lysine (50 µg/ml in PBS) coated 24-well culture plate and incubated overnight at 37°C and 5% CO_2. After 24 hours of incubation, the DMEM medium was replaced with freshly prepared NU-medium (Minimum Essential Medium (MEM) with 15% NU serum, 2% B27 supplement, 15 mM HEPES, 0.45% glucose, 1 mM sodium pyruvate, 2 mM GlutaMAX). Cultured neurons were transduced at 4 days *in vitro* (DIV4) with AAV-DJ-hSynapsin1-NOPLight.0 or NopLight-Ctr virus at a final titre of $4x10^9$ VG/ml culture media and imaged between DIV19–21. All reagents used are from Gibco. Unless otherwise noted, confocal imaging for all constructs reported in the manuscript are performed as follows:

Images were acquired on an inverted Zeiss LSM 800 microscope with a 488 nm laser for NOPLight and NOPLight-Ctr, and a 564 nm laser for Red-Dextran dye. For characterization of the dynamic range, expression level and pharmacological properties, HEK293T cells and/or neurons expressing the construct were first rinsed with HBSS (Life Technologies) and imaged at a final volume of 100 µL HBSS under a 40x objective. For pharmacological characterizations, the following compounds were used: Nocistatin (Abbiotec); J-113397 (Sigma-Aldrich); UFP-101 (Sigma-Aldrich); Ro 64-6198 (Sigma-Aldrich); MCOPPB (Cayman); Orphanin FQ (1-11) (Tocris); Leu-Enkephalin (Cayman); Met-Enkephalin (Cayman); Dynorphin A (Cayman); Dynorphin B (Cayman); β-Endorphin (Sigma-Aldrich); γ-Aminobutyric acid (Sigma-Aldrich); Dopamine hydrochloride (Sigma-Aldrich) and Acetylcholine bromide (Sigma-Aldrich). All compounds are diluted to the desired final concentration in HBSS before experiment except Ro 64-6198 and J-113397, which were diluted in <0.02% DMSO. All ligands were carefully pipetted into the imaging buffer during experiment. To determine the apparent affinity of the sensor, HEK293T cells and neurons cultured in glass bottom 24 well plates were rinsed with HBSS and imaged under a 20x objective with a final buffer volume of 500 µL HBSS. Ligands were manually applied on the cells during imaging to reach the desired final concentration.

$\Delta F/F_0$ was determined as the ratio of change in fluorescence signal change upon ligand activation and the baseline fluorescence level

$$\frac{\mathrm{F}_t - \mathrm{F}_0}{F_0}$$

where F_0 is determined as the mean intensity value over the baseline imaging period.

$$F_0 = \frac{1}{n}\sum_{t=0}^{t=n} F_t$$

Unless stated otherwise, only pixels corresponding to cell membrane were considered as regions of interest (ROIs) thus included in the analysis. ROIs were selected by auto-thresholding function of ImageJ and confirmed by visual inspection.

Kinetic measurements and analysis

To obtain the time constant for sensor activation, red fluorescent dye Antonia Red-Dextran (3000 M.W., Sigma-Aldrich) and N/OFQ (MedChem Express) were simultaneously applied in bolus to sensor-expressing HEK293T cells at 37°C with a stage top incubator (Tokai Hit). Fluorescent signals were excited at 488 nm (NOPLight) and 561 nm (Red-Dextran dye) and recorded using the high-speed line-scan function (Zeiss LSM 800) at 800Hz. The onset latency of each experiment was first determined by calculating the time for the red-dextran fluorescent signal to reach 85% percent of maximal value at the plateau. Only experiments with an onset latency smaller than 50 ms were considered in subsequent analysis to minimize the contribution of N/OFQ peptide diffusion to the temporal profile of sensor response. Membrane-corresponding pixels were first selected by thresholding pixel-wise $\Delta F/F_0$ at 65% criteria. Fluorescent signal change of each membrane pixel was then normalized and fitted by a mono-exponential association model using custom-written MATLAB script to derive the time constant τ.

One-photon spectral characterisation

One-photon fluorescence excitation (l_{em} = 560 nm) and emission (l_{exc} = 470 nm) spectra were determined using a Tecan M200 Pro plate reader at 37°C. HEK293T cells were transfected with Effectene transfection kit (QIAGEN). 24 hours after transfection cells were disscociated with Versene (Thermo Fisher) and thoroughly washed with PBS. Next, cells were resuspended in PBS to a final concentration of 3.3 x 10^6 cells/mL and aliquoted into two individual wells of a 96-well microplate with or without N/OFQ (1 uM), together with two wells containing the same amount of non-transfected cells to account for autofluorescence and a single well containing PBS to determine the Raman bands of the solvent.

Two-photon brightness characterisation

Two-photon brightness profiles of NOPLight were obtained from HEK293T cells before and after addition of N/OFQ (1 μM). Cells were transfected with Lipofectamine 3000 and were imaged 24 hours post transfection. The medium was replaced with PBS prior to imaging in order to avoid DMEM autofluorescence. The two-photon spectra were acquired as described previously[45].

cAMP assay

HEK293 cells growing at 70% confluency in a 10 cm dish were transfected with wild-type human NOPR or NOPLight (3 μg DNA) and GloSensor-20F (Promega, 2.5 μg DNA) using 12 μL Lipofectamine 2000 (Thermo Fisher) as in[71]. After 24 h, cells were plated into clear-bottom 96-well plates at 200,000 cells/well in DMEM (without phenol red, with 30 mM HEPES, p.H. 7.4) containing 250 μg/ml luciferin and incubated for 45-60 min at 37°C. Cells were treated with forskolin (3 μM) and varying concentrations of N/OFQ immediately followed by image acquisition every 45 s for 30 min at 37°C using a Hidex Sense plate reader. Luminescence values were normalized to the maximum luminescence values measured in the presence of 3 μM forskolin and to vehicle treated control cells.

TIRF microscopy

HEK293 cells growing on polylysine-coated 35 mm glass-bottom dishes (MatTek, P35G-1.5-14-C) were transfected with wild-type human NOPR or NOPLight (0.8 µg DNA) and β-arrestin-2-mCherry (1 µg DNA) using 3 µL Lipofectamine 2000 (Thermo Fisher). After 24 h, receptors were surface-labeled for 10 min with anti-FLAG M1-AF647[45] and media changed to HBS imaging solution (Hepes buffered saline (HBS) with 135 mM NaCl, 5 mM KCl, 0.4 mM $MgCl_2$,1.8 mM $CaCl_2$, 20 mM Hepes, 5 mM d-glucose adjusted to pH 7.4). Cells were imaged at 37°C using a Nikon TIRF microscope equipped with a 100x 1.49 oil CFI Apochromat TIRF objective, temperature chamber, objective heater, perfect focus system and an Andor DU897 EMCCD camera, in time-lapse mode with 10 s intervals. The laser lines used were 561 nm (for β-arrestin-2) and 647 nm (for receptor constructs). 10 µM N/OFQ was added by bath application. Protein relocalization (ΔF) was calculated as F(t)/F0 with F(t) being the β-arrestin-2 signal at each time point (t) (normalized to M1-AF647 signal, when specified) and F0 being the mean signal before ligand addition.

Virus production

The adeno associated virus (AAV) encoding NOPlight was produced by the Viral Vector Facility at the University of Zurich (VVF). The AAVs encoding the NOPlight-ctr sensor and the Cre-dependent NOPlight were produced by Vigene Biosciences. All other viruses used in this study were obtained either from the VVF or Addgene. The titers of the viruses used in this study were: AAVDJ-hSyn-NOPLight, $4.1x10^{13}$ GC/ml; AAVDJ-hSyn-NOPlight-ctr, $2.9x10^{13}$ GC/ml; AAVDJ-hSyn-FLEX-NOPlight, $2.5x10^{13}$ GC/ml; AAV5-EF1a-DIO-HA-hM3D(Gq)-mScarlet, $1.7x10^{13}$ GC/ml; AAV5-DIO-hSyn-mCherry, $2.4x10^{12}$ GC/ml; AAV8-hSyn-DIO-hM3Dq.mcherry, $1x10^{13}$ GC/ml.

Animals

10-24 week-old wild-type C57/Bl6 mice, PNOC-Cre (as described previously[22,23]) and OPRL1-Cre mice were used in this study. Animal procedures were approved and performed following

the local government authorities (Bezirksregierung Köln, Animal Care and Use Committee of University of Washington). Mice were housed at the animal facility at 22–24 °C and a 12 h/12 h light/dark cycle and ventilated cages receiving a standard chow and water ad libitum. Animals placed in the Pavlovian and operant conditioning paradigms were food restricted down to ~90% of their ad libitum body weight beginning one-week prior to conditioning for the entire duration of the paradigm.

Stereotaxic surgery

Viral vector injections and optic fiber implantation in the arcuate nucleus (ARC)

All surgeries were performed on male adult mice aged 8-10 weeks. Animals were anesthetized with 5% isoflurane and maintained at 1.5-2% throughout the surgery. For cell-specific DREADD expression, adeno-associated virus encoding AAV8-hSyn-DIO-hM3Dq.mcherry (Addgene #44361, 100 nL, viral titer 1 x 10^{13} GC/mL) was injected using a glass capillary into the ARC (-1.5 mm AP, -0.3 mm ML, -5.78 mm DV). Adeno-associated virus encoding AAV-DJ-hSyn-NOPLight (500 nL, viral titer 0.8 x 10^{13} GC/mL) was injected into the ARC in either wild-type or DREADD-expressing PNOC-Cre mice. All viruses were injected at a rate of 100 nL/min. For in vivo fiber photometry, after 5 minutes of viral injections a sterile optic fiber was implanted (diameter 400 µm, Doric Lenses) at the following coordinates (-0.450 mm AP, -0.2 mm ML, -5.545 mm DV) at an 8° angle. The implant was fixed with dental acrylic and closed with a cap after drying. Mice were allowed to recover from surgery 4 weeks before in vivo fiber photometry recordings started.

Viral vector injections and optic fiber implantation in the pnVTA

Following a minimum of seven days of acclimation to the holding facility, mice were initially anesthetized in an induction chamber (1-4% isoflurane) and placed into a stereotaxic frame (Kopf Instruments, Model 1900) where anesthesia was maintained at 1-2% isoflurane. Depending on the specific experimental paradigm, mice received viral injections either unilaterally or bilaterally using a blunt neural syringe (86200, Hamilton Company) at a rate of 100nL/min. For exogenous pharmacology experiments, wildtype (WT) mice were injected with AAV-DJ-hSyn-NOPLight (200-500nL, viral titer 2-4 x 10^{12} vg/mL) or AAV-DJ-hSyn-NOPLight-ctr (300nL, viral titer 2.9 x 10^{13} vg/mL) and OPRL1-Cre mice were injected with AAV-DJ-hSyn-Flex-NOPLight (300nL, viral titer 2.5 x 10^{13} vg/mL). For chemogenetic experiments, PNOC-Cre mice were co-injected with a 1:1 mix of AAV-DJ-hSyn-Flex-NOPLight (300nL, viral titer 2.5 x 10^{12} vg/mL) and either AAV5-EF1a-DIO-HA-hM3D(Gq)-mScarlet (300nL, viral titer 1.7 x 10^{13} vg/mL) or AAV5-DIO-hSyn-mCherry (300nL, viral titer 2.4 x 10^{12} vg/mL). For reward seeking behavioral experiments, WT mice were injected with AAV-DJ-hSyn-NOPLight (300nL, viral titer 4.1 x 10^{13} vg/mL). All viruses were injected into the VTA (stereotaxic coordinates from Bregma: -3.3 to -3.4 AP, +1.6 ML, -4.75 to -4.3 DV) at a 15° angle, with an optic fiber implanted above the injection site. Implants were secured using Metabond (C & B Metabond). Animals were allowed to recover from surgery for a minimum of 3 weeks before any behavioral testing, permitting optimal viral expression.

Acute brain slice preparation, electrophysiology and imaging

Experiments were performed at least 4 weeks after viral injections. The animals were lightly anesthetized with isoflurane (B506; AbbVie Deutschland GmbH and Co KG, Ludwigshafen, Germany) and decapitated. Coronal slices (280 µm) containing NOPLight expression in the arcuate nucleus (ARC) were cut with a vibration microtome (VT1200 S; Leica, Germany) under cold (4°C), carbogenated (95% O_2 and 5% CO_2), glycerol-based modified artificial cerebrospinal fluid (GaCSF: 244 mM Glycerol, 2.5 mM KCl, 2 mM MgCl2, 2 mM CaCl2, 1.2 mM NaH2PO4, 10 mM HEPES, 21 mM NaHCO3, and 5 mM Glucose adjusted to pH 7.2 with

NaOH). The brain slices were continuously perfused with carbogenated artificial cerebrospinal fluid (aCSF: 125 mM NaCl, 2.5 mM KCl, 2 mM $MgCl_2$, 2 mM $CaCl_2$, 1.2 mM NaH_2PO_4, 21 mM $NaHCO_3$, 10 mM HEPES, and 5 mM Glucose adjusted to pH 7.2 with NaOH) at a flow rate of ~2.5 ml/min. To reduce GABAergic and glutamatergic synaptic input, 10^{-4} M PTX (picrotoxin, P1675; Sigma-Aldrich), 5 x 10^{-6} M CGP (CGP-54626 hydrochloride, BN0597, Biotrend), 5 x 10^{-5} M DL-AP5 (DL-2-amino-5-phosphonopentanoic acid, BN0086, Biotrend), and 10^{-5} M CNQX (6-cyano-7-nitroquinoxaline-2,3-dione, C127; Sigma-Aldrich) were added to perfusion aCSF. The imaging setup consisted of a Zeiss AxioCam/MRm CCD camera with a 1388x1040 chip and a Polychromator V (Till Photonics, Gräfelfing, Germany) coupled via an optical fiber into the Zeiss Axio Examiner upright microscope. NOPLight fluorescence was collected at 470 nm excitation with 200 ms exposure time and a frame rate of 0.1 Hz. The emitted fluorescence was detected through a 500-550 nm bandpass filter (BP525/50), and data were acquired using 5x5 on-chip binning. Images were recorded in arbitrary units (AU) and analyzed as 16-bit grayscale images. To investigate the responses of NOPLight to N/OFQ (cat# 0910, Tocris), increasing concentrations (5 nM, 10 nM, 50 nM, 100 nM, 500 nM, 1 µM, 5 µM, 10 µM) of N/OFQ were sequentially bath-applied for 10 min each. Changes in fluorescent intensity upon ligand application were quantified by comparing the averaged fluorescent intensity measured in 3-minute intervals immediately before and at the end of ligand application. For electrophysiological recordings, the preparation of the brain slices and the recording conditions were the same as for the imaging experiments. Perforated patch clamp recordings were performed as previously described in[23]. To investigate NOPLight response to chemogenetically-evoked endogenous N/OFQ release, hM3Dq was activated by bath application of 3 µM clozapine N-oxide (CNO, ab141704, abcam) for 10 min. N/OFQ and CNO were bath-applied at a flow rate of ~2.5 ml/min. The analysis was performed offline using ImageJ (version 2.3.0/1.53f) and Prism 9 (GraphPad, California, USA). Amplitudes and kinetics of the signals were calculated as means (in AU) of fluorescent regions in the ARC, which were defined as the respective regions of interest (ROI, 0.15 – 0.2 mm^2). Biexponential fits of the signals' time courses before N/OFQ application were used to correct for bleaching.

Photometry Recording

Recordings in ARC

For fiber photometry studies in the arcuate nucleus, the set-up of the photometry recorder[72] consisted of an RZ5P real-time processor (Tucker-Davis Technologies) connected to a light source driver (LED Driver; Doric Lenses). The LED Driver constantly delivered excitation light at 405 nm (control) and 465 nm (NOPLight) wavelengths. The light sources were filtered by a four-port fluorescence minicube (FMC_AE(405)_E1(460-490)_F1(500-550)_S, Doric Lenses) before reaching the animal. The fluorescence signals were collected from the same fiber using a photoreceiver (Model 2151, New Focus), sent back to the RZ5P processor, and gathered by Synapse software (v.95-43718P, Tucker-Davis Technologies).

Recordings in pnVTA

For fiber photometry studies in the pnVTA, recordings were made continuously throughout the entirety of the pharmacology (30-minute), chemogenetic (55-minute), and reward-seeking (60-minute) sessions. Prior to recording, an optic fiber was attached to the implanted fiber using a ferrule sleeve (Doric, ZR_2.5). Two LEDs were used to excite NOPLight. In pharmacology and reward-seeking experiments, a 531-Hz sinusoidal LED light (Thorlabs, LED light: M470F3; LED driver: DC4104) was bandpass filtered (470 ± 20 nm, Doric, FMC4) to excite NOPLight and evoke NOPR-agonist dependent emission while a 211-Hz sinusoidal LED light (Thorlabs, M405FP1; LED driver: DC4104) was bandpass filtered (405 ± 10 nm, Doric, FMC4) to excite NOPLight and evoke NOPR-agonist independent isosbestic control emission. In chemogenetics experiments, a 531-Hz sinusoidal LED light (Thorlabs, LED light: M490F3; LED driver: DC4104) was bandpass filtered (490 ± 20 nm, Doric, FMC6) to excite NOPLight and evoke NOPR-agonist dependent emission while a 211-Hz sinusoidal LED light (Doric, CLED_435; Thorlabs, LED driver: DC4104) was bandpass filtered (435 ± 10 nm, Doric, FMC6) to excite NOPLight and evoke NOPR-agonist independent isosbestic control emission. Prior to recording, a 120s period of NOPLight excitation with either 470nm and 405nm or 490nm

and 435nm light was used to remove the majority of baseline drift. Power output for each LED was measured at the tip of the optic fiber and adjusted to ~ 30 μW before each day of recording. NOPLight fluorescence traveled back through the same optic fiber before being bandpass filtered (525 ± 25 nm, Doric, FMC4 or FMC6), detected with a photodetector system (Doric, DFD_FOA_FC), and recorded by a real-time processor (TDT, RZ5P). The 531-Hz and 211-Hz signals were extracted in real time by the TDT program Synapse at a sampling rate of 1017.25 Hz.

Data Analysis for Photometry Recordings

Recordings in ARC

Fiber photometry data was pre-processed by downsampling the raw data to 1 Hz and removing the first and last seconds of each recording to avoid noise. To correct for bleaching, the fluorescence decay as the baseline (F_0) for both signal and control channel were fitted using a Power-like Model[47]. If no model could be fitted for a sample (e.g. no decay), median of the baseline recording was used as a substitute. The relative change post-injection ($\Delta F/F_0$) was estimated by ($\Delta F_t/F_0 = (F_t - F_0)/F_0$) for both the signal and control channel separately (where F_t is the raw signal at time *t*). $\Delta F/F_{0control}$ was subsequently subtracted from ($\Delta F/F_{0signal}$ to correct for motion artifacts, obtaining a final estimate of the relative change in fluorescence intensity for each sample.

Recordings in pnVTA

Custom MatLab scripts were developed for analyzing fiber photometry data in the context of mouse behavior. A linear least squares (LLS) fit was applied to the control signal (405 or 435 nm) to align and fit it to the excitation signal (470 or 490 nm). For pharmacology and chemogenetics experiments where the entire length of the recording was analyzed to evaluate long-term changes in NOPLight fluorescence following drug injection, LLS fit was calculated using the recording's 'baseline' period that preceded the injection (5-10 minutes) while in reward-seeking and stress-related experiments where short event windows were evaluated,

LLS fit was calculated over the entire session. The fitted isosbestic signal was then subtracted from the excitation signal to detrend bleaching and remove movement artefacts from the NOPR-agonist dependent NOPLight fluorescence. To reduce high-frequency noise, data were down-sampled by a factor of 300. In pharmacology and chemogenetics experiments, the processed fiber photometry trace was smoothed across a rolling 10s window, and z-scored relative to the mean and standard deviation of the baseline period preceding drug injection (first 5 or 10 minutes of the recording, respectively). In reward-seeking and stress-related experiments decay from bleaching was first detrended by fitting a 5th degree polynomial function to the raw signal and isosbestic traces and subtracting the resulting curve, prior to performing the LLS fit described above. The processed traces were then smoothed across a rolling 1s window, extracted in windows surrounding the onset of relevant behavioral events (e.g., nose poke, cue onset, reward delivery, toe pinch), z-scored relative to the mean and standard deviation of each event window, and then averaged. The post-processed fiber photometry signal was analyzed in the context of animal behavior during Pavlovian conditioning and operant task performance.

Tissue preparation and immunohistochemistry (IHC)

IHC in the ARC

Brain slices were fixed in Roti-Histofix (PO873, Carl Roth) for ~12 h at 4°C and subsequently rinsed in 0.1 M phosphate-buffered saline (PBS, 3 x 10 min). PBS contained (in mM) 72 Na_2HPO_4 x dihydrate, 28 NaH_2PO_4 monohydrate, resulting in pH 7.2. To facilitate antibody penetration and prevent unspecific antibody binding, brain slices were preincubated in PBS containing 1% (w/v) Triton X-100 (TX, A1388, AppliChem) and 10% (v/v) normal goat serum (NGS, ENG9010-10, Biozol Diagnostica) for 30 min at room temperature (RT). Brain slices were then incubated for ~20 h at RT with primary antibodies (chicken anti-GFP, 1:1000, ab13970, Abcam; rat anti-mcherry, 1:1000, Thermo Fisher Scientific, M11217) in PBS-based blocking solution containing 0.1% TX, 10% NGS and 0.001% sodium azide (S2002, Sigma-

Aldrich). Brain slices were rinsed first in PBS-0.1% TX (2 x 10 min, RT), then in PBS (3 x 10 min, RT) and subsequently incubated with secondary antibodies (goat anti-chicken-FITC, Jackson #103-095-155, 1:500; goat anti-rabbit Alexa-Fluor-594, Thermo Fisher Scientific, A11012; 1:500) and DAPI (1:1000) for 2 hours at toom temperature. Brain slices were then rinsed in PBS-0.1% TX (2 x 10 min, RT) and PBS (3 x 10 min, RT), dehydrated in an ascending ethanol series, cleared with xylene (131769.1611, AppliChem), and mounted for imaging.

IHC in the pnVTA

Animals were transcardially perfused with 0.1M phosphate-buffered saline (PBS) followed by 40mL 4% paraformaldehyde (PFA). Brains were extracted and post-fixed in 4% PFA overnight and then transferred to 30% sucrose in PBS for cryoprotection. Brains were sectioned at 30μm on a microtome and stored in a 0.1M phosphate buffer at 4°C prior to immunohistochemistry. For behavioral cohorts, viral expression and optical fiber placements were confirmed before inclusion in the presented datasets. Immunohistochemistry was performed as previously described[73,74]. In brief, free-floating sections were washed in 0.1M PBS for 3 x 10-minute intervals. Sections were then placed in blocking buffer (0.5% Triton X-100 and 5% natural goat serum in 0.1M PBS) for 1 hour at room temperature. After blocking buffer, sections were placed in primary antibody (chicken anti-GFP, 1:2000, Abcam) overnight at 4°C. After 3 x 10-minute 0.1M PBS washes, sections were incubated in secondary antibody (AlexaFluor 488 goat anti-chicken, Abcam) for 2 hours at room temperature, followed by another round of washes (3 x 10 minutes in 0.1M PBS, 3 x 10 minutes in 0.1M PB). After immunostaining, sections were mounted and coverslipped with Vectashield HardSet mounting medium containing DAPI (Vector Laboratories) and imaged on a Leica DM6 B microscope.

In vivo animal experiments

All animal behaviors were performed within a sound-attenuated room maintained at 23°C at least one week after habituation to the holding room. Animals were handled for a minimum of

three days prior to experimentation, as well as habituated to the attachment of a fiber photometry patch cord to their fiber implants. For all experiments, mice were brought into the experimental room and allowed to acclimate to the space for at least 30 minutes. All experiments were conducted in red light to accommodate the reverse light cycle schedule, unless otherwise stated. All pharmacological interventions were administered in a counterbalanced manner. All sessions were video recorded.

In vivo pharmacology experiments in the ARC

Mice injected with AAV-DJ-hSyn-NOPLight were acclimatized to the behavior set-up 3 weeks post-surgery for one week. Awake animals were placed individually in a box and an optic fiber cable was connected to the implanted fiber. The optic fiber was attached to a swivel joint above the box to avoid moving limitations. Recording started 5 minutes after optic fiber tethering. A 10-minute-long baseline was recorded prior to the i.p. injection of vehicle or RO 64-6198 (different doses). Animals have no access to water or food during the recording session.

In vivo pharmacology experiments in the pnVTA

WT mice injected with either AAV-DJ-hSyn-NOPLight (n = 16) or AAV-DJ-hSyn-CtrNOPLight (n = 6) and OPRL1-Cre mice injected with AAV-DJ-hSyn-Flex-NOPLight (n = 3) were allowed to recover a minimum of 3 weeks after surgery. Three days before testing they were habituated to handling, fiber photometry cable attachment, and to the behavioral test box. On test day, animals were placed into the behavioral test box, which was a 10” x 10” clear acrylic box with a layer of bedding on the floor illuminated by a dim, diffuse white light (~30 lux). Fiber photometry recordings were made using a 405nm LED as the isosbestic channel and a 470nm LED as the signal channel. After starting the photometry recording, the mice were free to move around the box with no intervention for 5 minutes to establish a baseline photometry signal. At 5 minutes into the recording, NOPLight mice (n = 16) were scruffed and received an intraperitoneal (i.p.) injection of vehicle or 1, 5, or 10 mg/kg of the selective NOPR agonist Ro

64-6198 and were recorded for an additional 25 minutes. NOPLight-ctr and Flex NOPLight mice received an i.p. injection of 10 mg/kg Ro 64-6198 5 minutes into the recording. Two subsets of the NOPLight animals were recorded on three separate, counterbalanced days (at least 24 hours apart). The first subset (n = 4) received either i) an i.p. injection of 10 mg/kg Ro 64-6198 5 minutes into the recording (RO), ii) an oral gavage (o.g.) treatment with 10 mg/kg of selective NOPR antagonist LY-2940094 5 minutes into the recording (LY), or iii) an o.g. treatment with 10 mg/kg LY-2940094 30 minutes prior to the recording followed by an i.p. injection with 10 mg/kg Ro 64-6198 5 minutes into the recording (LY pretreatment + Ro). The second subset (n = 4-9) received either i) an i.p. injection of 10 mg/kg Ro 64-6198 5 minutes into the recording (RO), ii) an i.p. injection of 10 mg/kg of selective NOPR antagonist J-113397 5 minutes into the recording (J11), or iii) an i.p. injection of 10 mg/kg J-113397 30 minutes prior to the recording followed by an i.p. injection with 10 mg/kg Ro 64-6198 5 minutes into the recording (J11 pretreatment + Ro).

In vivo chemogenetics (DREADD) experiments

PNOC-Cre mice co-injected with AAV-DJ-hSyn-Flex-NOPLight and either AAV5-EF1a-DIO-HA-hM3D(Gq)-mScarlet (n = 8) or AAV5-DIO-hSyn-mCherry (n = 3) were allowed to recover a minimum of 3 weeks after surgery. Three days before testing they were habituated to handling, fiber photometry cable attachment, and to the behavioral test box. On test day, animals were placed into the behavioral test box, which was a 10” x 10” clear acrylic box with a layer of bedding on the floor illuminated by a dim, diffuse white light (~30 lux). Fiber photometry recordings were made using a 435nm LED as the isosbestic channel and a 490nm LED as the signal channel. After starting the photometry recording, the mice were free to move around the box with no intervention for 10 minutes to establish a baseline photometry signal. At 10 minutes into the recording, mice were scruffed and received an intraperitoneal (i.p.) injection of 5 mg/kg clozapine-N-oxide (CNO) and were recorded for an additional 45 minutes. A subset of the DIO hM3D(Gq) animals (n = 3) were recorded on two separate, counterbalanced days (at least 24 hours apart). On one recording day, they received the CNO

treatment and recording timeline described above. On the other recording day, they were administered an oral gavage (o.g.) treatment with 10 mg/kg of the selective NOPR antagonist LY-2940094 30 minutes prior to the photometry recording. The LY-pretreatment group then underwent the same recording timeline and CNO injection (5 mg/kg i.p., after a 10-minute baseline) as they did on the CNO only day.

Reward-seeking (Pavlovian, operant) conditioning paradigms

One week prior to Pavlovian conditioning, WT fiber photometry mice expressing AAV-DJ-hSyn-NOPLight in the VTA (n = 4) were food restricted down to ~90% of their free feeding body weight. All reward-seeking training was completed in Med-Associates operant conditioning boxes (ENV-307A). Fiber photometry recordings were made using a 405nm LED as the isosbestic channel and a 470nm LED as the signal channel. Mice were first trained to associate illumination of a house light (CS, 5 seconds) with delivery of a single sucrose pellet (US) occurring immediately after the house light turned off. A randomized intertrial interval of between 30-120s separated consecutive trials. Pavlovian conditioning sessions lasted for 60 minutes, over which an averaged of 36-38 rewards were presented. Pavlovian conditioning was repeated over 5 days a total of 5 times, with simultaneous fiber photometry recordings made during session 1 and session 4. Animals were then moved onto a fixed ratio 1 (FR1) schedule for 5 days (60 minutes/session), where they were required to perform a nosepoke in the active nosepoke port one time to receive the 5-second house light cue and subsequent pellet delivery. Pokes made into the inactive port had no effect. Simultaneous fiber photometry recordings were made during FR1 sessions 1 and 4. Following FR1 training, the ratio was increased to an FR3 schedule for 4 days (60 minutes/session) requiring the mice to perform 3 active port nosepokes to receive the house light cue and a sucrose pellet, with simultaneous photometry recording during session 3. Last, mice were placed in a single, 120-minute session on a progressive ratio schedule (PR) where the nosepoke criteria for each subsequent reward delivery followed the geometric progression $n_i = 5e^{i/5} - 5$ (1, 2, 4, 6, 9, 12…), increasing in an exponential manner. Mice were removed from food restriction immediately upon completion

of the PR test, and 24 days later were re-tested in a single, 60-minute FR1 session. For this session, fiber photometry recordings were made using a 435nm LED as the isosbestic channel and a 490nm LED as the signal channel.

Stress-related behavior

WT mice injected with AAV-DJ-hSyn-NOPLight (n = 5) and implanted with a stainless-steel head-ring to allow for head-fixation during fiber photometry recording were allowed to recover a minimum of 3 weeks after surgery. For the four days prior to testing, animals were habituated to handling, fiber photometry cable attachment, and head-fixation. During testing, animals were head-fixed to minimize motion-related artefacts in the fiber photometry signal. Fiber photometry recordings were made over two counterbalanced sessions using 405nm and 470nm LEDs for one session, and 435nm and 490nm LEDs for the other. During a single session, mice received four acute toe pinches to the right hind paw separated by a two-minute intertrial interval.

Statistical analyses

All data were averaged and expressed as mean ± SEM. Statistical significance was taken as *$p < 0.05$, ** $p < 0.01$, ***$p < 0.001$, and ****$p < 0.0001$, as determined by Mann-Whitney test, Wilcoxon test, two-way repeated-measures ANOVA followed by Bonferroni post hoc tests as appropriate. All n values for each experimental group are described in the corresponding figure legend. For behavioral experiments, group size ranged from n = 3 to n = 16. Statistical analyses were performed in GraphPad Prism 9 (Graphpad, La Jolla, CA) and MATLAB 9.9 (The MathWorks, Natick, MA).

References

1. Meunier, J.-C. *et al.* Isolation and structure of the endogenous agonist of opioid receptor-like ORL1 receptor. *Nature* **377**, 532–535 (1995).
2. Reinscheid, R. K. *et al.* Orphanin FQ: A Neuropeptide That Activates an Opioidlike G Protein-Coupled Receptor. *Science* **270**, 792–794 (1995).
3. Wang, Y. *et al.* Structures of the entire human opioid receptor family. *Cell* S0092867422015458 (2023) doi:10.1016/j.cell.2022.12.026.
4. Thompson, A. A. *et al.* Structure of the Nociceptin/Orphanin FQ Receptor in Complex with a Peptide Mimetic. *Nature* **485**, 395–399 (2012).
5. Toll, L., Bruchas, M. R., Calo', G., Cox, B. M. & Zaveri, N. T. Nociceptin/Orphanin FQ Receptor Structure, Signaling, Ligands, Functions, and Interactions with Opioid Systems. *Pharmacol. Rev.* **68**, 419–457 (2016).
6. Berthele, A. *et al.* [3H]-nociceptin ligand-binding and nociceptin opioid receptor mrna expression in the human brain. *Neuroscience* **121**, 629–640 (2003).
7. Neal, C. R. *et al.* Localization of orphanin FQ (nociceptin) peptide and messenger RNA in the central nervous system of the rat. *J. Comp. Neurol.* **406**, 503–547 (1999).
8. Mollereau, C. & Mouledous, L. Tissue distribution of the opioid receptor-like (ORL1) receptor. *Peptides* **21**, 907–917 (2000).
9. Andero, R. Nociceptin and the nociceptin receptor in learning and memory. *Prog. Neuropsychopharmacol. Biol. Psychiatry* **62**, 45–50 (2015).
10. Moulédous, L. The Nociceptin/Orphanin FQ System and the Regulation of Memory. *Handb. Exp. Pharmacol.* **254**, 259–278 (2019).
11. Schultz, W. Dopamine reward prediction-error signalling: a two-component response. *Nat. Rev. Neurosci.* **17**, 183–195 (2016).
12. Wise, R. A. Dopamine, learning and motivation. *Nat. Rev. Neurosci.* **5**, 483–494 (2004).
13. McCutcheon, J. E., Ebner, S. R., Loriaux, A. L. & Roitman, M. F. Encoding of Aversion by Dopamine and the Nucleus Accumbens. *Front. Neurosci.* **6**, 137 (2012).
14. Murphy, N. P., Ly, H. T. & Maidment, N. T. Intracerebroventricular orphanin FQ/nociceptin suppresses dopamine release in the nucleus accumbens of anaesthetized rats. *Neuroscience* **75**, 1–4 (1996).
15. Olianas, M. C., Dedoni, S., Boi, M. & Onali, P. Activation of nociceptin/orphanin FQ-NOP receptor system inhibits tyrosine hydroxylase phosphorylation, dopamine synthesis, and dopamine D1 receptor signaling in rat nucleus accumbens and dorsal striatum. *J. Neurochem.* **107**, 544–556 (2008).
16. Di Giannuario, A. & Pieretti, S. Nociceptin differentially affects morphine-induced dopamine release from the nucleus accumbens and nucleus caudate in rats. *Peptides* **21**, 1125–1130 (2000).
17. Lutfy, K., Do, T. & Maidment, N. T. Orphanin FQ/nociceptin attenuates motor stimulation and changes in nucleus accumbens extracellular dopamine induced by cocaine in rats. *Psychopharmacology (Berl.)* **154**, 1–7 (2001).
18. Ciccocioppo, R., Angeletti, S., Panocka, I. & Massi, M. Nociceptin/orphanin FQ and drugs of abuse. *Peptides* **21**, 1071–1080 (2000).
19. Chiou, L.-C. *et al.* Nociceptin/orphanin FQ peptide receptors: pharmacology and clinical implications. *Curr. Drug Targets* **8**, 117–135 (2007).
20. Civelli, O. The orphanin FQ/nociceptin (OFQ/N) system. *Results Probl. Cell Differ.* **46**, 1–25 (2008).

21. Sakoori, K. & Murphy, N. P. Endogenous nociceptin (orphanin FQ) suppresses basal hedonic state and acute reward responses to methamphetamine and ethanol, but facilitates chronic responses. *Neuropsychopharmacol. Off. Publ. Am. Coll. Neuropsychopharmacol.* **33**, 877–891 (2008).
22. Parker, K. E. *et al.* A Paranigral VTA Nociceptin Circuit that Constrains Motivation for Reward. *Cell* **178**, 653-671.e19 (2019).
23. Jais, A. *et al.* PNOCARC Neurons Promote Hyperphagia and Obesity upon High-Fat-Diet Feeding. *Neuron* **106**, 1009-1025.e10 (2020).
24. Driscoll, J. R., Wallace, T. L., Mansourian, K. A., Martin, W. J. & Margolis, E. B. Differential Modulation of Ventral Tegmental Area Circuits by the Nociceptin/Orphanin FQ System. *eNeuro* **7**, ENEURO.0376-19.2020 (2020).
25. Walker, J. R., Terenius, L. & Koob, G. F. Conditioned opioid withdrawal decreases nociceptin/orphanin FQ levels in the frontal cortex and olfactory tubercle. *Neuropsychopharmacol. Off. Publ. Am. Coll. Neuropsychopharmacol.* **27**, 203–211 (2002).
26. Ciccocioppo, R. *et al.* NOP-Related Mechanisms in Substance Use Disorders. *Handb. Exp. Pharmacol.* **254**, 187–212 (2019).
27. Ciccocioppo, R. *et al.* Restraint Stress Alters Nociceptin/Orphanin FQ and CRF Systems in the Rat Central Amygdala: Significance for Anxiety-Like Behaviors. *J. Neurosci.* **34**, 363–372 (2014).
28. Kuzmin, A., Kreek, M. J., Bakalkin, G. & Liljequist, S. The Nociceptin/Orphanin FQ Receptor Agonist Ro 64-6198 Reduces Alcohol Self-Administration and Prevents Relapse-Like Alcohol Drinking. *Neuropsychopharmacology* **32**, 902–910 (2007).
29. Rorick-Kehn, L. M. *et al.* A Novel, Orally Bioavailable Nociceptin Receptor Antagonist, LY2940094, Reduces Ethanol Self-Administration and Ethanol Seeking in Animal Models. *Alcohol. Clin. Exp. Res.* **40**, 945–954 (2016).
30. Gavioli, E. C., Rae, G. A., Calo', G., Guerrini, R. & De Lima, T. C. M. Central injections of nocistatin or its C-terminal hexapeptide exert anxiogenic-like effect on behaviour of mice in the plus-maze test. *Br. J. Pharmacol.* **136**, 764–772 (2002).
31. Jenck, F. *et al.* Orphanin FQ acts as an anxiolytic to attenuate behavioral responses to stress. *Proc. Natl. Acad. Sci. U. S. A.* **94**, 14854–14858 (1997).
32. Varty, G. B. *et al.* The Anxiolytic-Like Effects of the Novel, Orally Active Nociceptin Opioid Receptor Agonist 8-[bis(2-Methylphenyl)methyl]-3-phenyl-8-azabicyclo[3.2.1]octan-3-ol (SCH 221510). *J. Pharmacol. Exp. Ther.* **326**, 672–682 (2008).
33. Al-Hasani, R. *et al.* In vivo detection of optically-evoked opioid peptide release. *eLife* **7**, (2018).
34. Jaquins-Gerstl, A. & Michael, A. C. A review of the effects of FSCV and microdialysis measurements on dopamine release in the surrounding tissue. *The Analyst* **140**, 3696–3708 (2015).
35. Wu, Z., Lin, D. & Li, Y. Pushing the frontiers: tools for monitoring neurotransmitters and neuromodulators. *Nat. Rev. Neurosci.* **23**, 257–274 (2022).
36. Sabatini, B. L. & Tian, L. Imaging Neurotransmitter and Neuromodulator Dynamics In Vivo with Genetically Encoded Indicators. *Neuron* **108**, 17–32 (2020).
37. Labouesse, M. A. & Patriarchi, T. A versatile GPCR toolkit to track in vivo neuromodulation: not a one-size-fits-all sensor. *Neuropsychopharmacology* 1–5 (2021) doi:10.1038/s41386-021-00982-y.

38. Ravotto, L., Duffet, L., Zhou, X., Weber, B. & Patriarchi, T. A bright and colorful future for G-protein coupled receptor sensors. *Front. Cell. Neurosci.* **14**, (2020).
39. Wu, Z. *et al.* Neuronal activity-induced, equilibrative nucleoside transporter-dependent, somatodendritic adenosine release revealed by a GRAB sensor. *Proc. Natl. Acad. Sci.* **120**, e2212387120 (2023).
40. Patriarchi, T. *et al.* Ultrafast neuronal imaging of dopamine dynamics with designed genetically encoded sensors. *Science* **360**, eaat4422 (2018).
41. Sun, F. *et al.* A Genetically Encoded Fluorescent Sensor Enables Rapid and Specific Detection of Dopamine in Flies, Fish, and Mice. *Cell* **174**, 481-496.e19 (2018).
42. Patriarchi, T. *et al.* Ultrafast neuronal imaging of dopamine dynamics with designed genetically encoded sensors. *Science* **360**, eaat4422 (2018).
43. Bockaert, J., Marin, P., Dumuis, A. & Fagni, L. The 'magic tail' of G protein-coupled receptors: an anchorage for functional protein networks. *FEBS Lett.* **546**, 65–72 (2003).
44. Malfacini, D. *et al.* Pharmacological Profile of Nociceptin/Orphanin FQ Receptors Interacting with G-Proteins and β-Arrestins 2. *PLOS ONE* **10**, e0132865 (2015).
45. Duffet, L. *et al.* A genetically encoded sensor for in vivo imaging of orexin neuropeptides. *Nat. Methods* **19**, 231–241 (2022).
46. Donica, C. L., Awwad, H. O., Thakker, D. R. & Standifer, K. M. Cellular Mechanisms of Nociceptin/Orphanin FQ (N/OFQ) Peptide (NOP) Receptor Regulation and Heterologous Regulation by N/OFQ. *Mol. Pharmacol.* **83**, 907–918 (2013).
47. Gunaydin, L. A. *et al.* Natural neural projection dynamics underlying social behavior. *Cell* **157**, 1535–1551 (2014).
48. Lerner, T. N. *et al.* Intact-Brain Analyses Reveal Distinct Information Carried by SNc Dopamine Subcircuits. *Cell* **162**, 635–647 (2015).
49. Post, A. *et al.* A Selective Nociceptin Receptor Antagonist to Treat Depression: Evidence from Preclinical and Clinical Studies. *Neuropsychopharmacol. Off. Publ. Am. Coll. Neuropsychopharmacol.* **41**, 1803–1812 (2016).
50. Hardaway, J. A. *et al.* Central Amygdala Prepronociceptin-Expressing Neurons Mediate Palatable Food Consumption and Reward. *Neuron* **102**, 1037-1052.e7 (2019).
51. Witkin, J. M. *et al.* The biology of Nociceptin/Orphanin FQ (N/OFQ) related to obesity, stress, anxiety, mood, and drug dependence. *Pharmacol. Ther.* **141**, 283–299 (2014).
52. Rodriguez-Romaguera, J. *et al.* Prepronociceptin-Expressing Neurons in the Extended Amygdala Encode and Promote Rapid Arousal Responses to Motivationally Salient Stimuli. *Cell Rep.* **33**, 108362 (2020).
53. Morairty, S. R., Sun, Y., Toll, L., Bruchas, M. R. & Kilduff, T. S. Activation of the nociceptin/orphanin-FQ receptor promotes NREM sleep and EEG slow wave activity. *Proc. Natl. Acad. Sci. U. S. A.* **120**, e2214171120 (2023).
54. Devine, D. P., Hoversten, M. T., Ueda, Y. & Akil, H. Nociceptin/orphanin FQ content is decreased in forebrain neurones during acute stress. *J. Neuroendocrinol.* **15**, 69–74 (2003).
55. Green, M. K. & Devine, D. P. Nociceptin/orphanin FQ and NOP receptor gene regulation after acute or repeated social defeat stress. *Neuropeptides* **43**, 507–514 (2009).
56. Duffet, L. *et al.* A genetically encoded sensor for in vivo imaging of orexin neuropeptides. *Nat. Methods* **19**, 231–241 (2022).
57. Conway, S. M., Mikati, M. O. & Al-Hasani, R. Challenges and new opportunities for detecting endogenous opioid peptides in reward. *Addict. Neurosci.* **2**, 100016 (2022).

58. Sandberg, M. & Weber, S. G. Techniques for neuropeptide determination. *Trends Anal. Chem. TRAC* **22**, 522–527 (2003).
59. Girven, K. S., Mangieri, L. & Bruchas, M. R. Emerging approaches for decoding neuropeptide transmission. *Trends Neurosci.* **45**, 899–912 (2022).
60. van den Pol, A. N. Neuropeptide transmission in brain circuits. *Neuron* **76**, 98–115 (2012).
61. Journigan, V. B., Polgar, W. E., Khroyan, T. V. & Zaveri, N. T. Designing bifunctional NOP receptor-mu opioid receptor ligands from NOP-receptor selective scaffolds. Part II. *Bioorg. Med. Chem.* **22**, 2508–2516 (2014).
62. Kallupi, M. *et al.* Genetic Deletion of the Nociceptin/Orphanin FQ Receptor in the Rat Confers Resilience to the Development of Drug Addiction. *Neuropsychopharmacol. Off. Publ. Am. Coll. Neuropsychopharmacol.* **42**, 695–706 (2017).
63. Norton, C. S., Neal, C. R., Kumar, S., Akil, H. & Watson, S. J. Nociceptin/orphanin FQ and opioid receptor-like receptor mRNA expression in dopamine systems. *J. Comp. Neurol.* **444**, 358–368 (2002).
64. Flau, K., Redmer, A., Liedtke, S., Kathmann, M. & Schlicker, E. Inhibition of striatal and retinal dopamine release via nociceptin/orphanin FQ receptors. *Br. J. Pharmacol.* **137**, 1355–1361 (2002).
65. Khan, M. S., Boileau, I., Kolla, N. & Mizrahi, R. A systematic review of the role of the nociceptin receptor system in stress, cognition, and reward: relevance to schizophrenia. *Transl. Psychiatry* **8**, 38 (2018).
66. Duffet, L. *et al.* Optical tools for visualizing and controlling human GLP-1 receptor activation with high spatiotemporal resolution. 2023.02.14.528498 Preprint at https://doi.org/10.1101/2023.02.14.528498 (2023).
67. Wu, Z. *et al.* A sensitive GRAB sensor for detecting extracellular ATP in vitro and in vivo. *Neuron* S0896627321009880 (2021) doi:10.1016/j.neuron.2021.11.027.
68. Jing, M. *et al.* An optimized acetylcholine sensor for monitoring in vivo cholinergic activity. *Nat. Methods* **17**, 1139–1146 (2020).
69. Qian, T. *et al.* A genetically encoded sensor measures temporal oxytocin release from different neuronal compartments. *Nat. Biotechnol.* 1–14 (2023) doi:10.1038/s41587-022-01561-2.
70. Meng, C. *et al.* Spectrally Resolved Fiber Photometry for Multi-component Analysis of Brain Circuits. *Neuron* **98**, 707-717.e4 (2018).
71. Zhang, N. R. *et al.* Serine 363 Is Required for Nociceptin/Orphanin FQ Opioid Receptor (NOPR) Desensitization, Internalization, and Arrestin Signaling. *J. Biol. Chem.* **287**, 42019–42030 (2012).
72. Porniece Kumar, M. *et al.* Insulin signalling in tanycytes gates hypothalamic insulin uptake and regulation of AgRP neuron activity. *Nat. Metab.* **3**, 1662–1679 (2021).
73. Al-Hasani, R., McCall, J. G., Foshage, A. M. & Bruchas, M. R. Locus Coeruleus Kappa-Opioid Receptors Modulate Reinstatement of Cocaine Place Preference Through a Noradrenergic Mechanism. *Neuropsychopharmacology* **38**, 2484–2497 (2013).
74. Kim, T. *et al.* Injectable, cellular-scale optoelectronics with applications for wireless optogenetics. *Science* **340**, 211–216 (2013).
75. Baek, M. *et al.* Accurate prediction of protein structures and interactions using a three-track neural network. *Science* **373**, 871–876 (2021).

DATA AVAILABILITY

DNA and protein sequences for the new sensors developed in this study have been deposited on the National Center for Biotechnology Information database (accession nos. OQ067483 and OQ067484) and are available in Supplementary Data S1. DNA plasmids used for viral production have been deposited both on the UZH Viral Vector Facility (https://vvf.ethz.ch/) and on Addgene. Viral vectors can be obtained either from the Patriarchi laboratory, the UZH Viral Vector Facility, or Addgene. All source data are provided with the manuscript. All other raw data can be made available upon reasonable request.

CODE AVAILABILITY

Custom MATLAB code is available on https://github.com/patriarchilab/NOPLight.

ACKNOWLEDGEMENTS

The results are part of a project that has received funding from the European Research Council (ERC) under the European Union's Horizon 2020 research and innovation program (Grant agreement No.s 891959 and 101016787 to TP; 742106 to JCB). We also acknowledge funding from the University of Zürich Forschungskredit (FK-20-042, XZ), the Swiss National Science Foundation (Grant No. 310030_196455, TP; PCEFP3_181282, MS), the NIMH P50MH119467 (MRB), and the Deutsche Forschungsgemeinschaft (401832153, 431549029, EXC 2030-390661388, P.K). We would like to thank Jean-Charles Paterna and the Viral Vector Facility of the Neuroscience Center Zürich (ZNZ) for the kind help with virus production.

Author contributions

TP and MRB led the study. XZ, CS, TP, and MRB conceptualized and designed the study. XZ developed the NOPLight and NOPLight-ctr sensors, performed in vitro sensor screening and characterization, including confocal imaging in HEK293T cells and neurons, under the supervision of TP. MAB prepared primary neuronal cultured under supervision of DB. JD performed two-photon spectral characterization under the supervision of LR, TP and BW. KA performed signaling assays under the supervision of MS. DF and PK performed and analysed acute brain slice electrophysiology and imaging experiments. POP, CAB and LS performed and analysed in vivo photometry data in arcuate nucleus under supervision of JCB. CS performed and analysed in vivo photometry and chemogenetic experiments in the pnVTA under the supervision of MRB. ASA, JCJ, SJ helped with surgeries and behavioural animal training for experiments in pnVTA under the supervision of MRB. TP, MRB, XZ and CS wrote the manuscript with contributions from all authors.

COMPETING FINANCIAL INTERESTS

T.P. is a co-inventor on a patent application related to the technology described in this article. All other authors have nothing to disclose.

Figure Legends

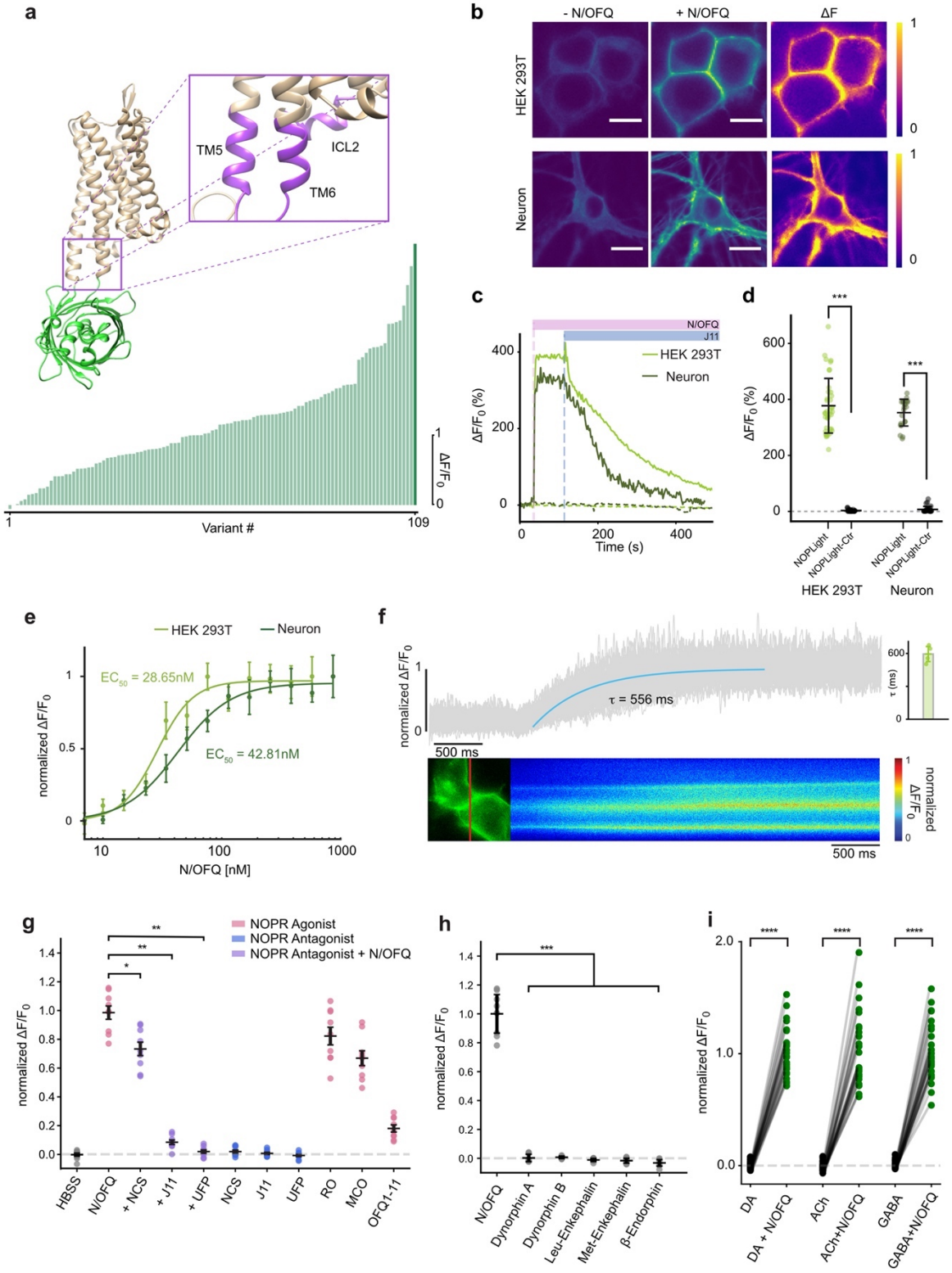

Figure 1. Development and in vitro characterization of NOPLight.
a. Upper left: RoseTTAFold[75] predicted structural model of NOPLight. Upper right: zoom in of receptor and cpGFP linker region. Residues of site-directed mutagenesis highlighted in purple. Lower panel: Summary of maximal $\Delta F/F_0$ in response to 10 μM N/OFQ of HEK293T cells expressing each of the 109 variants screened in this study. (n ≥ 3 cells for each variant. Dark green bar: NOPLight). **b.** Representative images of HEK 293T cells (top; scale bars, 10 μm) and neurons (bottom; scale bars, 20 μm) expressing NOPLight before (left) and after (middle) application of 1 μM N/OFQ. Corresponding normalized pixelwise ΔF shown on the right. **c.** Representative fluorescent-fold change ($\Delta F/F_0$) of HEK 293T cell (light green traces) and neurons (dark green traces) expressing NOPLight (solid line) or NOPLight-Ctr (dotted line) in response to 1 μM N/OFQ, followed by competition of 10 μM J-113397, a NOPR antagonist. **d.** Quantification of maximal $\Delta F/F_0$ of NOPLight (green) or NOPLight-Ctr (gray) expressing HEK293T cells and neurons in response to 1 μM N/OFQ. (n = 38, 30, 22, 27 cells from >3 independent experiments, left to right respectively. Data shown as mean ± s.t.d.) ***P<0.0001. P = 1.003×10^{-12} and 1.262×10^{-9} (One-sided Mann-whitney U test) for the response of NOPLight compared to NOPLight-Ctr in HEK 293T cells and neurons. **e.** Normalized maximal $\Delta F/F_0$ response of HEK 293T cells (light green) and neurons (dark green) expressing NOPLight to different concentrations of N/OFQ (Data shown as mean ± s.d.) and respective dose response curve fitted with a three parameter Hill equation. n = 3 independent experiments with > 5 cells each. **f.** time plot of normalized single NOPLight pixel $\Delta F/F_0$ (gray) from a representative line-scan (upper right). Pixel average $\Delta F/F_0$ were fitted with a mono-exponential function (blue trace) and the deduced time constant (τ). Corresponding cell image (red: line scanned) and time profile of all pixels on the line scanned are shown directly under the time plot. Upper right inset: quantification of time constant (τ) from four independent experiments. **g.** Maximal $\Delta F/F_0$ response in NOPLight expressing HEK293T cells to the application of different drug(s) (NCS: Nocistatin; J11: J-113397; UFP: UFP-101; RO: Ro 64-6198; MCO: MCOPPB; OFQ1-11: Orphanin FQ (1-11)). Response to N/OFQ in the presence of each antagonist was compared to where only N/OFQ was applied by a pairwise Mann-Whitney rank test with post hoc Bonferroni correction (*P<0.01, **P<0.005.P = 0.024, Nocistatin; 0.0012, J113397; 0.0012, UFP 101;) **h.** Maximal $\Delta F/F_0$ response in NOPLight expressing HEK293T cells to the application of endogenous opioid ligands (1 μM). Response to each ligand was compared to the response to N/OFQ by a pairwise Mann-Whitney rank test with post hoc Bonferroni correction (**P<0.005, P = 0.003, Dynorphin A; 0.003, Dynorphin B; 0.003, Leu-Enkephalin ; 0.003, Met-Enkephalin ; 0.003, β-endorphin.) **i.** Maximal $\Delta F/F_0$ response in NOPLight expressing HEK293T cells to the application of fast neurotransmitters (DA: dopamine, ACh: acetylcholine, GABA: gamma-Aminobutyric acid at 1 mM) normalized to its maximal $\Delta F/F_0$ response to N/OFQ (1 μM). n = 29-30 cells from 3 independent experiments. ****P<0.0001.

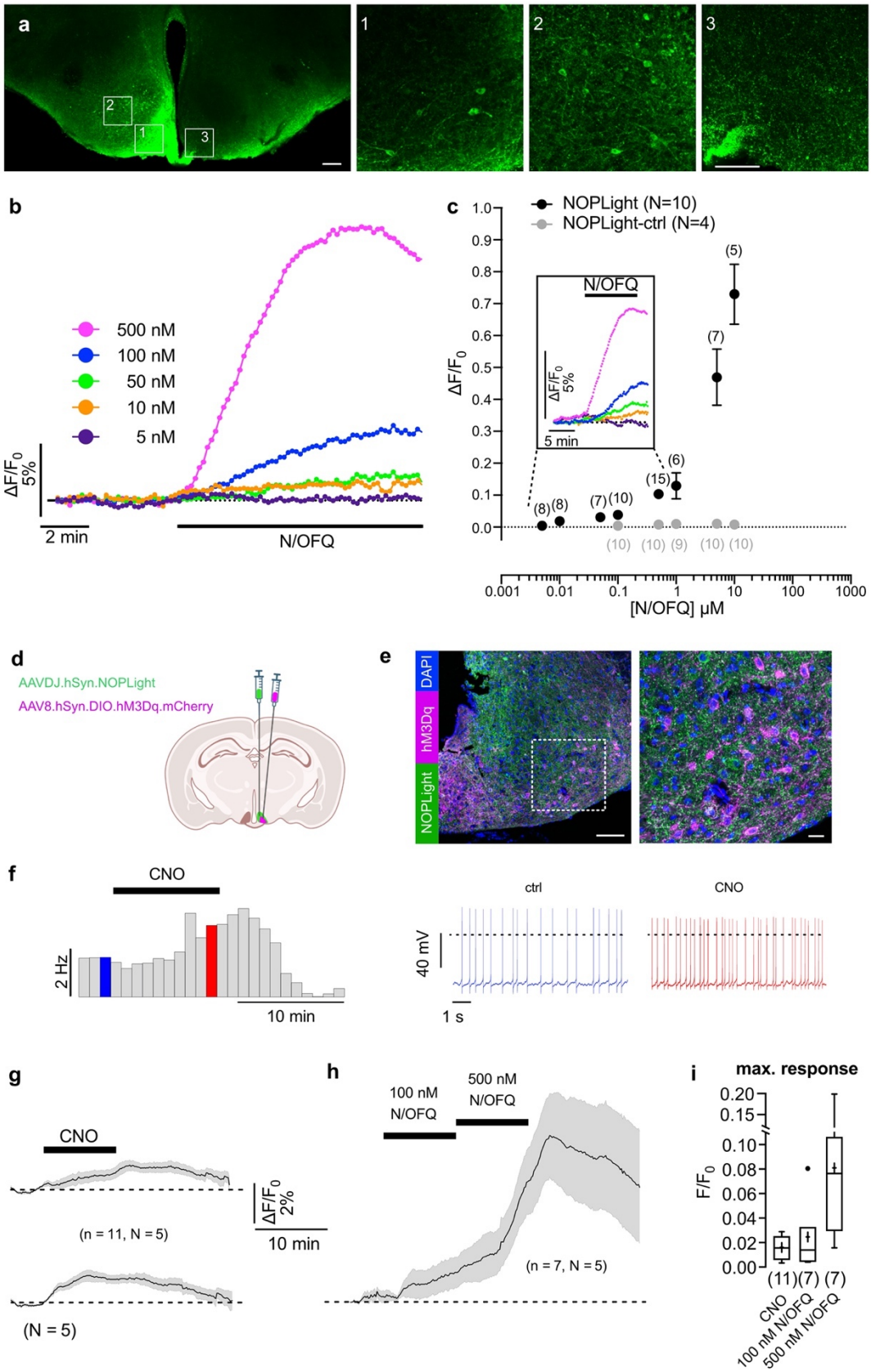
a
1
2
3
b
500 nM
100 nM
50 nM
10 nM
5 nM
ΔF/F0
5%
2 min
N/OFQ
c
NOPLight (N=10)
NOPLight-ctrl (N=4)
N/OFQ
ΔF/F0
5%
5 min
ΔF/F0
[N/OFQ] μM
d
AAVDJ.hSyn.NOPLight
AAV8.hSyn.DIO.hM3Dq.mCherry
e
DAPI
hM3Dq
NOPLight
f
CNO
2 Hz
10 min
ctrl
CNO
40 mV
1 s
g
CNO
ΔF/F0
2%
10 min
(n = 11, N = 5)
(N = 5)
h
100 nM
N/OFQ
500 nM
N/OFQ
(n = 7, N = 5)
i
max. response
F/F0
CNO
100 nM N/OFQ
500 nM N/OFQ

Figure 2. Ex vivo characterization of NOPLight.
a. Expression of NOPLight in the ARC. Scale bar, 200 µm. Insets, scale bars, 50 µm. **b-f.** Change in NOPLight fluorescence measured in ARC neurons in response to bath-applied N/OFQ or release of chemogenetically-activated PNOC neurons. The fluorescence was detected from 0.15 – 0.2 mm^2 ROIs in the ARC. Each experiment was performed in a different brain slices. **b.** NOPLight responses of a single ROI to increasing N/OFQ concentrations. **c.** Concentration-response relation showing the N/OFQ (black trace) effect on N/OFQ fluorescence of NOPLight-expressing cells in the ARC. The grey trace shows the concentration-response relation for the ligand insensitive mutant sensor (NOPLight-ctr, grey trace). Data are shown as mean ± SEM. Inset, mean fluorescence increase in response to different concentrations of N/OFQ. Color code as in **b**. ARC, arcuate nucleus of the hypothalamus. **d.** Experimental schematic for chemogenetic experiments in brain slices. **e.** Representative immunohistochemical image showing DREADD (hM3Dq) expression in PNOC neurons of the ARC as well as pan-neuronal expression of NOPLight. Scale bar, 100 µm. Magnification of inset is shown on right. Scale bar, 20 µm. **f.** Perforated patch clamp recordings from a hM3Dq-expressing PNOC neuron showing the effect of 10 min CNO application (3 µM) on action potential frequency. Left, rate histogram (bin width 60s). Right, representative sections of the original recording corresponding to the times indicated by blue and red color code. **g-i.** Changes (mean ± SEM) in NOPLight fluorescence measured in the ARC in response to activation of hM3Dq-expressing PNOC neurons by 10 min bath-application of 3 µM clozapine N-oxide (CNO) (**g**) and 100 nM and 500 nM N/OFQ (**h**). **g.** The upper and lower panel show the same data. The traces in the upper panel are aligned to the CNO application, the traces in the lower panel are aligned to the response onset. The recordings in **g** and **h** were performed from the same brain slices. The n-values in **h** are lower than in **g** because some recordings were terminated for technical reasons. Bars indicate the application of CNO and N/OFQ, respectively. Scale bars apply to **g** and **h**. **i.** Box plots showing the maximal fluorescence changes upon applications of CNO and N/OFQ, respectively. The numbers in brackets represents the numbers of experiments (brain slices). N-values indicate the number of animals.

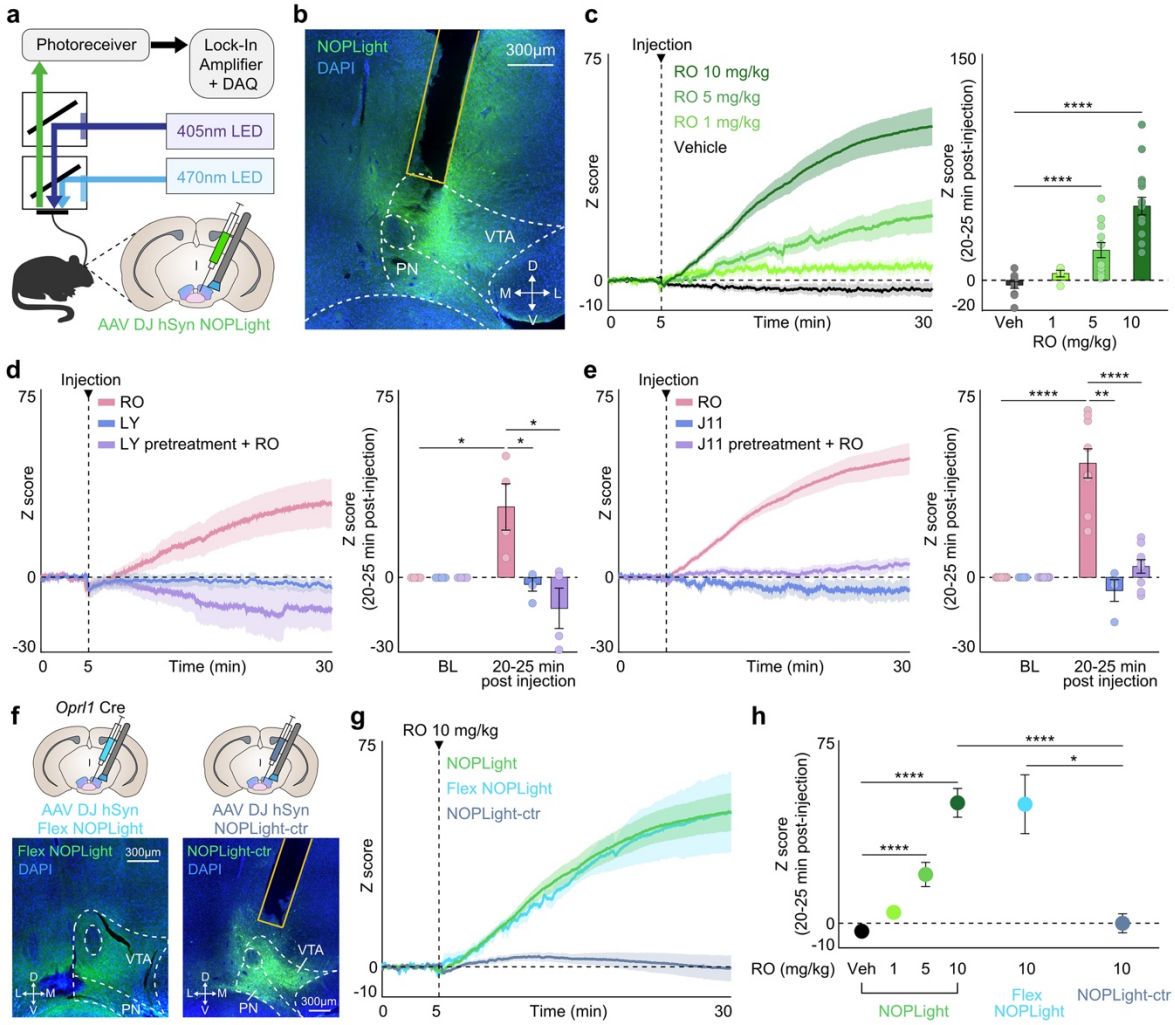
a
Photoreceiver
Lock-In Amplifier + DAQ
405nm LED
470nm LED
AAV DJ hSyn NOPLight
b
NOPLight
DAPI
300µm
VTA
PN
c
Injection
RO 10 mg/kg
RO 5 mg/kg
RO 1 mg/kg
Vehicle
Z score
Time (min)
Z score (20-25 min post-injection)
RO (mg/kg)
Veh
d
RO
LY
LY pretreatment + RO
BL
20-25 min post injection
e
J11
J11 pretreatment + RO
f
Oprl1 Cre
AAV DJ hSyn Flex NOPLight
AAV DJ hSyn NOPLight-ctr
Flex NOPLight
NOPLight-ctr
g
RO 10 mg/kg
NOPLight
Flex NOPLight
NOPLight-ctr
h
RO (mg/kg)
NOPLight
Flex NOPLight
NOPLight-ctr

Figure 3. Characterization of NOPLight response in vivo to pharmacological agonism and antagonism.
a. Schematic of fiber photometry setup. Coronal brain cartoon of viral injection of NOPLight and fiber implant in the VTA. **b.** Representative image showing expression of DAPI (blue) and NOPLight (green) with fiber placement in VTA. **c.** Left: Averaged traces of NOPLight fluorescence after systemic (i.p.) injection of vehicle (black) or 1, 5, or 10 mg/kg of selective NOPR agonist Ro 64-6198. Right: Mean NOPLight fluorescence 20-25 minutes after Ro 64-6198 injection increases dose-dependently (two-tailed Mann-Whitney test, ****$p<0.0001$, n = 5-16 mice). Data represented as mean ± SEM **d.** Left: Averaged traces of NOPLight fluorescence after systemic injection of Ro 64-6198 (i.p.) and/or 10 mg/kg of selective NOPR antagonist LY2940094 (o.g.). LY2940094 was administered to the LY + RO group 30 min prior to photometry recording. Right: NOPR antagonist pre-treatment blocks Ro 64-6198 induced increases in NOPLight fluorescence (two-tailed Mann-Whitney test, *$p<0.05$, n = 4 mice). Data represented as mean ± SEM **e.** Left: Averaged traces of NOPLight fluorescence after systemic (i.p.) injection of Ro 64-6198 and/or 10 mg/kg of selective NOPR antagonist J113397. J113397 was administered to the J11 + RO group 30 min prior to photometry recording Right: NOPR antagonist pre-treatment blocks Ro 64-6198 induced increases in NOPLight fluorescence (two-tailed Mann-Whitney test, **$p<0.01$, ****$p<0.0001$, n = 4-9 mice). Data represented as mean ± SEM **f.** Top: Coronal brain cartoon of viral injection of Flex-NOPLight (left) or NOPLight-ctr (right) and fiber implant in the VTA. Bottom: Representative image showing expression of DAPI (blue) and Flex-NOPLight (left, green) or NOPLight-ctr (right, green) with fiber placement in VTA. **g.** Averaged traces of NOPLight (green), Flex-NOPLight (blue) or Ctr-NOPLight (gray) fluorescence after systemic (i.p.) injection of 10 mg/kg Ro 64-6198 (n = 3-16 mice). Data represented as mean ± SEM **h.** Mean fluorescence of each NOPLight variant 20-25 min after systemic injection of Ro 64-6198 (two-tailed Mann-Whitney test, *$p<0.05$, ****$p<0.0001$, n = 3-16 mice). Data represented as mean ± SEM.

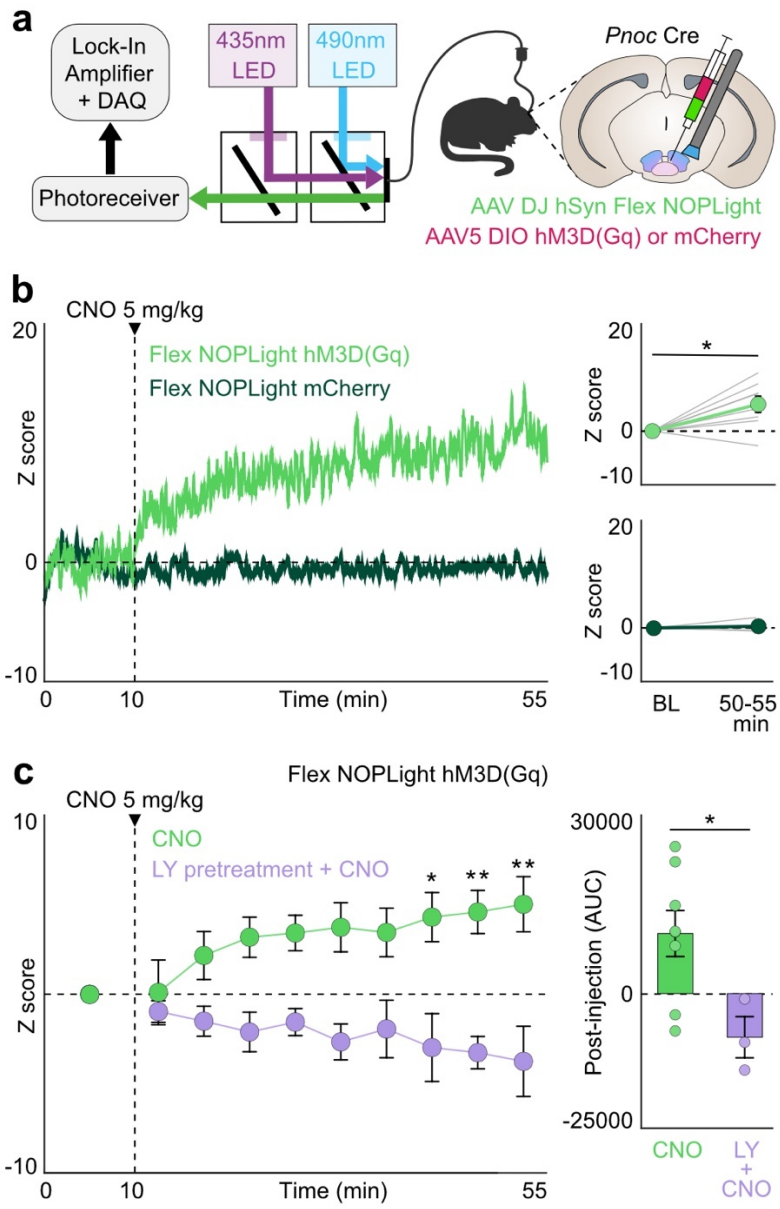
a
Lock-In Amplifier + DAQ
435nm LED
490nm LED
Photoreceiver
Pnoc Cre
AAV DJ hSyn Flex NOPLight
AAV5 DIO hM3D(Gq) or mCherry
b
CNO 5 mg/kg
Flex NOPLight hM3D(Gq)
Flex NOPLight mCherry
Z score
Time (min)
BL
50-55 min
c
Flex NOPLight hM3D(Gq)
CNO 5 mg/kg
CNO
LY pretreatment + CNO
Post-injection (AUC)
LY + CNO

Figure 4. NOPLight detects chemogenetically evoked endogenous N/OFQ release *in vivo*.

a. Schematic of fiber photometry setup. Coronal brain cartoon of viral co-injection of Flex-NOPLight with either DIO-hM3D(Gq) or mCherry and fiber implant in the VTA of PNOC Cre mice. **b.** Left: Representative traces of Flex-NOPLight fluorescence after systemic (i.p.) injection of 5 mg/kg CNO in hM3D(Gq) (green) or control (red) animals. Right: Mean Flex-NOPLight fluorescence 40-45 minutes after CNO injection is significantly elevated relative to pre-injection baseline period (BL) in hM3D(Gq) but not control mice (two-tailed Wilcoxon test, *$p<0.05$, n = 8 mice, hM3D(Gq); 3 mice, control). Data represented as mean ± SEM **c.** Left: Flex-NOPLight fluorescence averaged before injection (i.p.) of 5 mg/kg CNO (0-10 min), and in 5 min bins following the injection.10 mg/kg of selective NOPR antagonist LY2940094 was administered (o.g.) to the LY + CNO group 30 min prior to photometry recording (two-way repeated-measures ANOVA with Bonferroni's post hoc test, *$p<0.05$, **$p<0.01$, n = 3-8 mice). Right: NOPR antagonist pre-treatment prevents CNO induced increases in Flex-NOPLight fluorescence (two-tailed Mann-Whitney test, *$p<0.05$). Data represented as mean ± SEM.

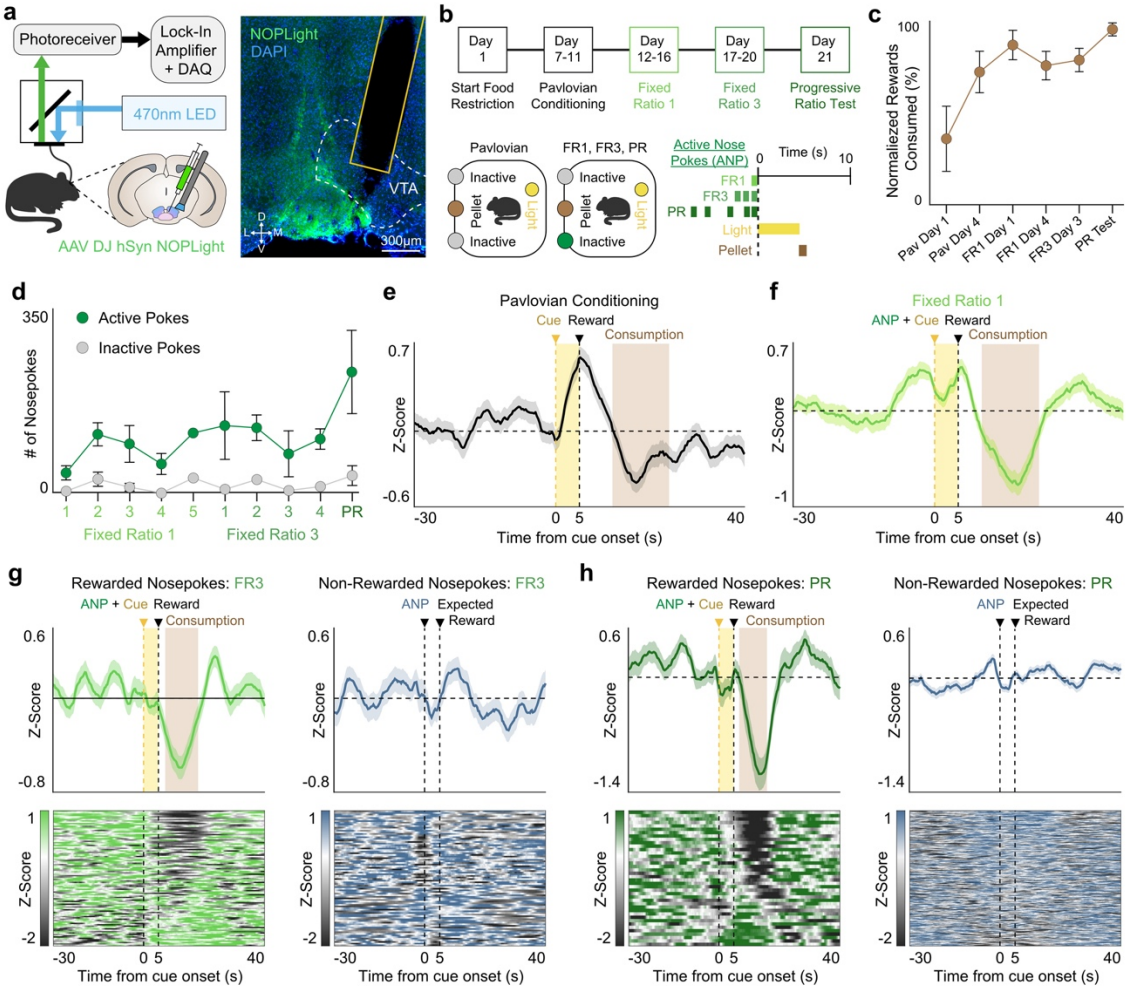
a
Photoreceiver
Lock-In Amplifier + DAQ
470nm LED
AAV DJ hSyn NOPLight
NOPLight
DAPI
VTA
300µm
b
Day 1
Day 7-11
Day 12-16
Day 17-20
Day 21
Start Food Restriction
Pavlovian Conditioning
Fixed Ratio 1
Fixed Ratio 3
Progressive Ratio Test
Pavlovian
FR1, FR3, PR
Inactive
Pellet
Light
Active Nose Pokes (ANP)
Time (s)
FR1
FR3
PR
Light
Pellet
c
Normalized Rewards Consumed (%)
Pav Day 1
Pav Day 4
FR1 Day 1
FR1 Day 4
FR3 Day 3
PR Test
d
Active Pokes
Inactive Pokes
# of Nosepokes
Fixed Ratio 1
Fixed Ratio 3
e
Pavlovian Conditioning
Cue
Reward
Consumption
Z-Score
Time from cue onset (s)
f
Fixed Ratio 1
ANP + Cue
Reward
Consumption
Z-Score
Time from cue onset (s)
g
Rewarded Nosepokes: FR3
ANP + Cue
Reward
Consumption
Non-Rewarded Nosepokes: FR3
ANP
Expected Reward
Z-Score
Time from cue onset (s)
h
Rewarded Nosepokes: PR
ANP + Cue
Reward
Consumption
Non-Rewarded Nosepokes: PR
ANP
Expected Reward
Z-Score
Time from cue onset (s)

Figure 5: NOPLight detection of endogenous VTA N/OFQ release during Pavlovian and operant conditioning.
a. Left: Schematic of fiber photometry setup. Coronal brain cartoon of viral injection of NOPLight and fiber implant in the VTA of WT mice (n = 4). Right: Representative image showing expression of DAPI (blue) and NOPLight (green) with fiber placement in VTA. **b.** Top: Timeline depicting training regimen for Pavlovian conditioning and operant conditioning. Bottom: Cartoon depicting operant box setup and trial structure for each training paradigm. **c.** Proportion of delivered rewards that were consumed by the mice on each of the photometry recording days. Data represented as mean ± SEM **d.** Total number of nosepokes made in the active (green) or inactive (gray) nosepoke ports across the entire training regimen. Data represented as mean ± SEM **e.** Trace of mean NOPLight signal during the reward period of a single Pavlovian conditioning session, aligned to start of light cue (yellow, shaded). Time to pellet retrieval and duration of consumption period averaged across all trials and animals (brown, shaded). Data represented as mean ± SEM **f.** Trace of mean NOPLight signal during the reward period of a single fixed ratio 1 (FR1) session, aligned to active nosepokes. Time to pellet retrieval and duration of consumption period averaged across all trials and animals (brown, shaded). Data represented as mean ± SEM **g.** Left: Trace of mean NOPLight signal during the reward period of a single fixed ratio 3 (FR3) session, aligned to reinforced active nosepokes (top) with corresponding heat map (bottom). Each row corresponds to an individual FR3 reward period. Time to pellet retrieval and duration of consumption period averaged across all trials and animals (brown, shaded). Right: Trace of mean NOPLight signal during fixed ratio 3 (FR3) session, aligned to nonreinforced active nosepokes (top) with corresponding heat map (bottom). Each row corresponds to an individual, nonreinforced active nosepoke epoch. Data represented as mean ± SEM **h.** Left: Trace of mean NOPLight signal during the reward period of the progressive ratio (PR) test, aligned to reinforced active nosepokes (top) with corresponding heat map (bottom). Each row corresponds to an individual PR reward period. Time to pellet retrieval and duration of consumption period averaged across all trials and animals (brown, shaded). Right: Heat map of NOPLight fluorescence during PR session, aligned to nonreinforced active nosepokes (top) with corresponding heat map (bottom). Each row corresponds to an individual, nonreinforced active nosepoke epoch. Data represented as mean ± SEM.

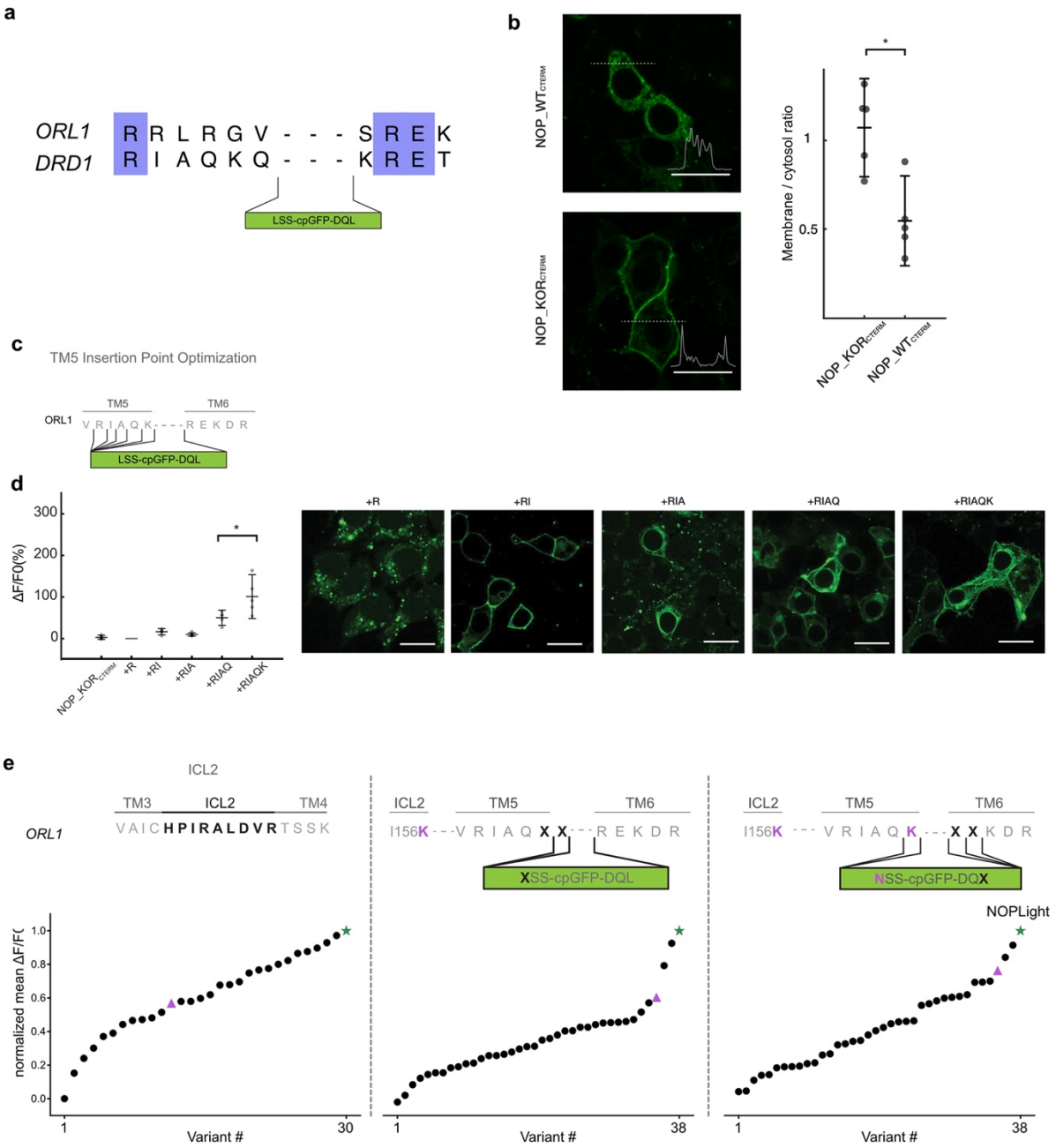
a
ORL1 R R L R G V - - - S R E K
DRD1 R I A Q K Q - - - K R E T
LSS-cpGFP-DQL
b
NOP_WTCTERM
NOP_KORCTERM
Membrane / cytosol ratio
1
0.5
*
NOP_KORCTERM
NOP_WTCTERM
c
TM5 Insertion Point Optimization
TM5
TM6
ORL1 V R I A Q K - - - - R E K D R
LSS-cpGFP-DQL
d
ΔF/F0(%)
300
200
100
0
*
NOP_KORCTERM
+R
+RI
+RIA
+RIAQ
+RIAQK
+R
+RI
+RIA
+RIAQ
+RIAQK
e
ICL2
TM3
ICL2
TM4
ORL1
V A I C H P I R A L D V R T S S K
normalized mean ΔF/F(
1.0
0.8
0.6
0.4
0.2
0.0
1
30
Variant #
ICL2
TM5
TM6
I156K - - - V R I A Q X X - - - R E K D R
XSS-cpGFP-DQL
1
38
Variant #
ICL2
TM5
TM6
I156K - - - V R I A Q K - - - X X K D R
NSS-cpGFP-DQX
NOPLight
1
38
Variant #

Supplementary Figure 1. Development and optimization of NOPLight.
a. Sequence alignment of transmembrane domains (TM) 5 and 6 from ORL1 and DRD1 to determine the insertion site for the cpGFP module from dLight1.3. Color code indicates percent identity between the human NOPR and DRD1. **b.** Left: Representative images of membrane expression profile of HEK293T cells expressing *in silico* designed sensor prototype with a wild-type NOPR C-terminus ($N/OFQ_{_WTcterm}$) and a chimeric sensor with the C-terminus of kappa opioid receptor ($N/OFQ_{_KORcterm}$). Insets: fluorescent intensity of all pixels along the dotted line of each image. Scale bars, 10 μm. Right: Quantification of the ratio between pixel averaged fluorescent intensity of cell membrane and that of the cytosol. n = 5 cells. （P = 0.011, one-sided Mann Whitney U test） **c.** Schematic representation of the optimization of the insertion site at TM5 linker region. **d.** Left: Maximal $\Delta F/F_0$ response to 10 μM N/OFQ of all sensor prototypes shown in **c.** Right: representative image of HEK293T cells expressing sensor prototypes. **e.** Top: Schematic representation of three rounds of directed mutagenesis to improve sensor dynamic range. Amino acids that were mutated into a subset of different amino acids in the screening process are labelled in bold. Selected mutation from previous round of screening labelled in magenta. Bottom: Normalized $\Delta F/F_0$ response of HEK293T cells expressing each variant to 10 μM N/OFQ. Each data point represents averaged $\Delta F/F_0$ response from > 3 cells in 3 independent experiments normalized to the maximal $\Delta F/F_0$ response of the best variant in the current round of screening. Magenta: Selected variant from previous round of screening. Green: Best variant in current round of screening.

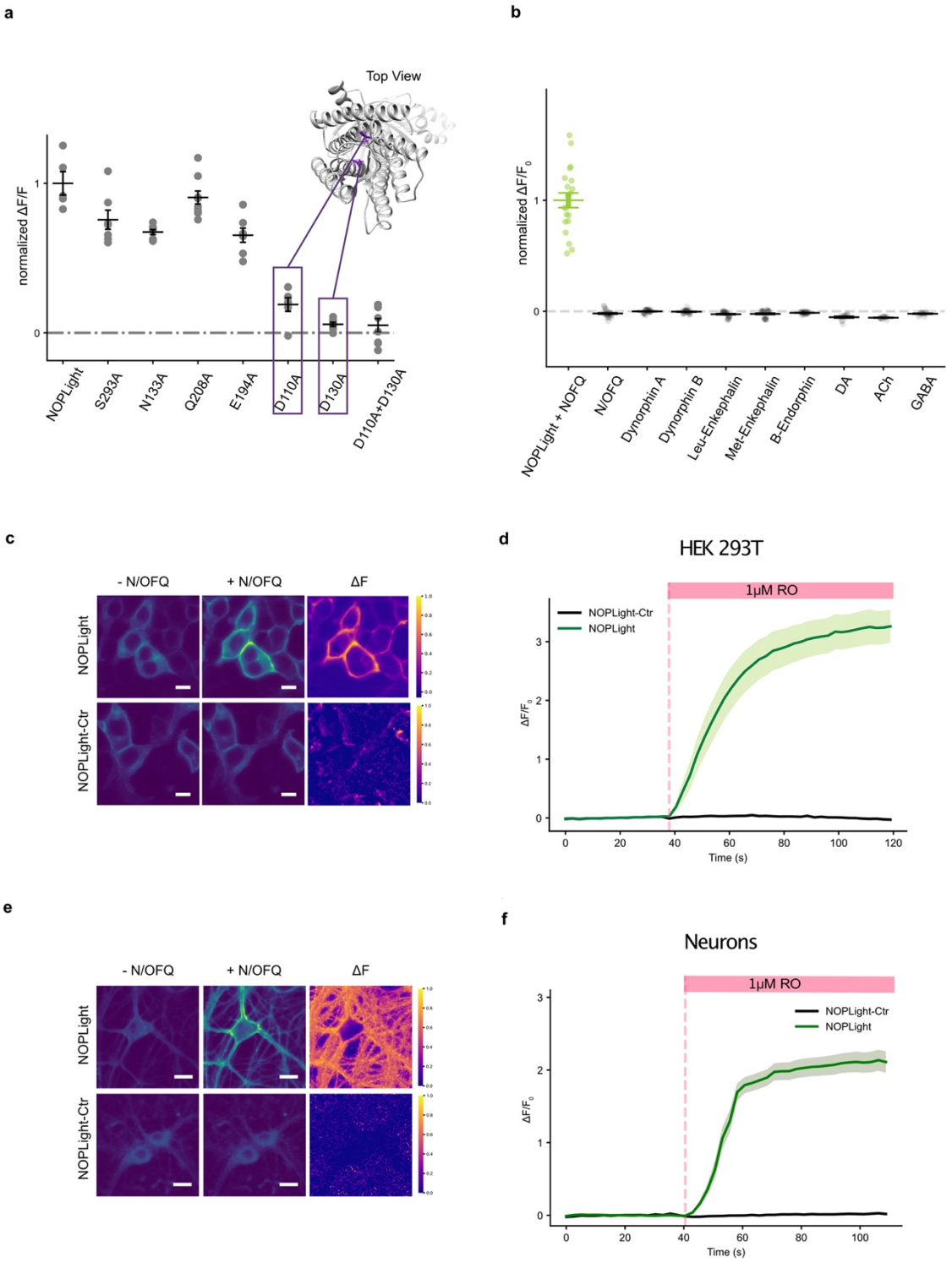
a
Top View
normalized ΔF/F
NOPLight
S293A
N133A
Q208A
E194A
D110A
D130A
D110A+D130A
b
normalized ΔF/F0
NOPLight + NOFQ
N/OFQ
Dynorphin A
Dynorphin B
Leu-Enkephalin
Met-Enkephalin
B-Endorphin
DA
ACh
GABA
c
- N/OFQ
+ N/OFQ
ΔF
NOPLight
NOPLight-Ctr
d
HEK 293T
1μM RO
NOPLight-Ctr
NOPLight
ΔF/F0
Time (s)
e
- N/OFQ
+ N/OFQ
ΔF
NOPLight
NOPLight-Ctr
f
Neurons
1μM RO
NOPLight-Ctr
NOPLight
ΔF/F0
Time (s)

Supplementary Figure 2. Development and characterisation of NOPLight-ctr.
a. Quantification of maximal $\Delta F/F_0$ in response to 10 µM N/OFQ in HEK 293T cells expressing NOPLight mutants. Mutated residues indicated by their absolute residue numbering in reference to human NOPR. Structural model of NOPLight-Ctr is predicted by RoseTTAfold[75]. The two mutations selected for NOPLight-ctr are highlighted in purple. **b.** Normalized maximal $\Delta F/F_0$ of NOPLight-Ctr-expressing HEK 293T cells in response to endogenous opioid peptides (1 µM) and fast neurotransmitters (DA: dopamine, Ach: acetylcholine, GABA: gamma-Aminobutyric acid (1 mM)). All data normalized to NOPLight-expressing HEK293T cells (green). **c.** Representative images of HEK 293T cells expressing NOPLight (top; scale bars, 10 µm) and NOPLight-Ctr (bottom; scale bars, 10 µm) before and after application of 1 µM Ro 64-6198. Corresponding normalized pixelwise ΔF shown on the right. **d.** Average fluorescent-fold change ($\Delta F/F_0$) of HEK 293T cell expressing NOPLight (light green trace) or NOPLight-Ctr (black trace) in response to 1 µM RO 64-6198 (3 experiments, data shown as mean + s.e.m). **e.** Representative images of neurons expressing NOPLight (top; scale bars, 20 µm) and NOPLight-Ctr (bottom; scale bars, 20 µm) before and after application of 1 µM Ro 64-6198. Corresponding normalized pixelwise ΔF shown on the right. **f.** Average fluorescent-fold change ($\Delta F/F_0$) of neurons expressing NOPLight (light green trace) or NOPLight-Ctr (black trace) in response to 1 µM RO 64-6198 (3 experiments, data shown as mean ± s.e.m).

a

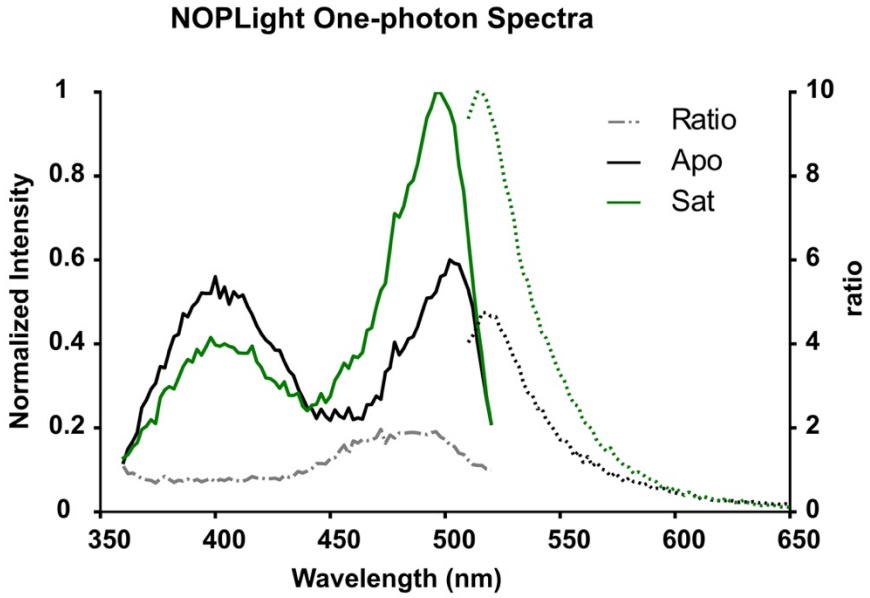
NOPLight One-photon Spectra
Normalized Intensity
ratio
Wavelength (nm)
Ratio
Apo
Sat
0
0.2
0.4
0.6
0.8
1
0
2
4
6
8
10
350
400
450
500
550
600
650

b

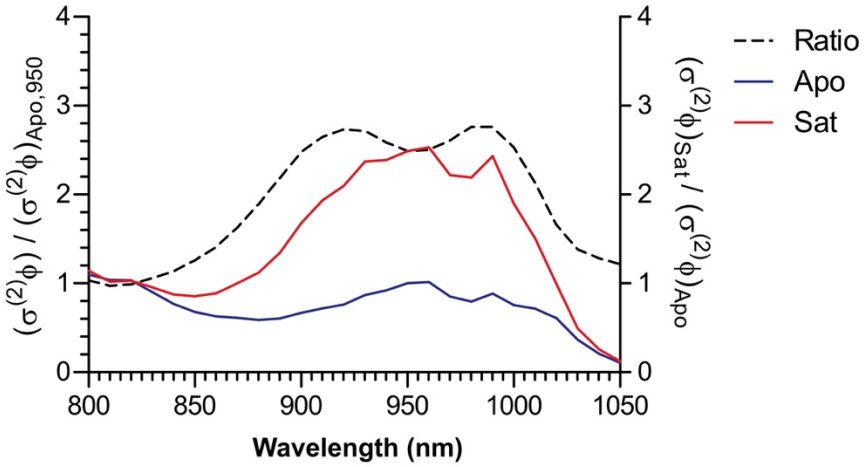
NOPLight Two-photon Spectra
$(\sigma^{(2)}\phi) / (\sigma^{(2)}\phi)_{Apo,950}$
$(\sigma^{(2)}\phi)_{Sat} / (\sigma^{(2)}\phi)_{Apo}$
Wavelength (nm)
Ratio
Apo
Sat
0
1
2
3
4
800
850
900
950
1000
1050

Supplementary Figure 3. Spectral properties of NOPLight.
a. Normalized one-photon fluorescence excitation (solid lines, $\lambda_{excitation}$ = 360 – 520 nm, $\lambda_{emission}$ = 560nm) and emission (dotted lines, $\lambda_{excitation}$ = 470 nm, $\lambda_{emission}$ = 510 – 650 nm) spectra of NOPLight-expressing HEK 293T cells in the absence and presence of N/OFQ (1 μM). Traces shown are averaged from 4 independent experiments. Intensity measured at each wavelength is normalized to the maximum intensities measured for both the excitation and emission spectra. **b.** Relative two-photon brightness of NOPLight imaged in transfected HEK cells grown attached to a glass coverslip in the presence (Sat) or absence (Apo) of N/OFQ (1 μM). Ratio between Sat and Apo shown in dashed line. Each trace is the average of 3 independent experiments.

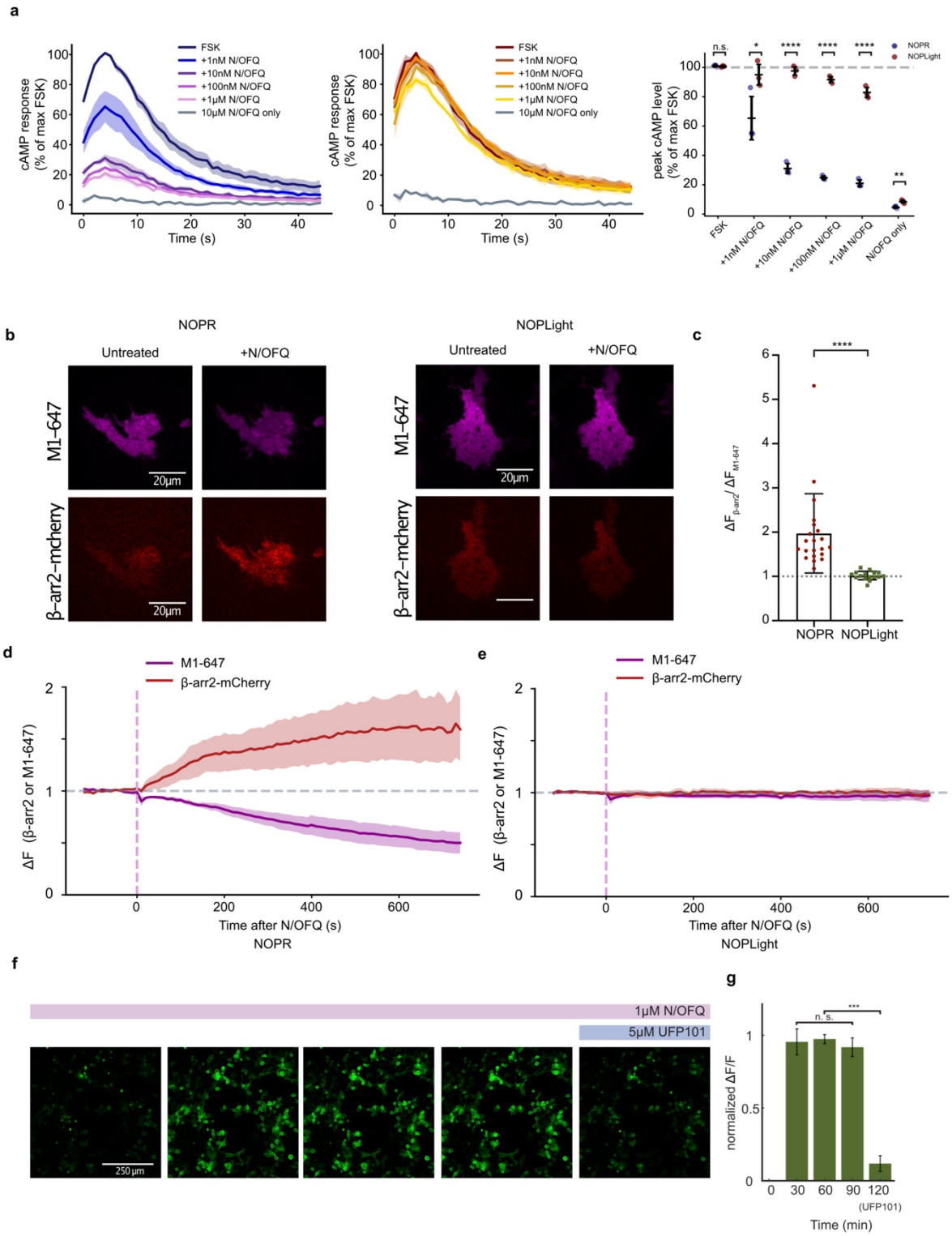
a
cAMP response (% of max FSK)
Time (s)
FSK
+1nM N/OFQ
+10nM N/OFQ
+100nM N/OFQ
+1μM N/OFQ
10μM N/OFQ only
peak cAMP level (% of max FSK)
NOPR
NOPLight
n.s.
FSK
+1nM N/OFQ
+10nM N/OFQ
+100nM N/OFQ
+1μM N/OFQ
N/OFQ only
b
NOPR
NOPLight
Untreated
+N/OFQ
M1-647
β-arr2-mcherry
20μm
c
NOPR
NOPLight
d
M1-647
β-arr2-mCherry
ΔF (β-arr2 or M1-647)
Time after N/OFQ (s)
NOPR
e
NOPLight
f
1μM N/OFQ
5μM UFP101
250 μm
g
normalized ΔF/F
Time (min)
(UFP101)

Supplementary Figure 4. Characterization of sensor coupling to intracellular signaling pathways.

a. Left: cAMP GloSensor luciferase activity traces in NOPR expressing HEK293 cells in response to different concentrations of N/OFQ, normalized to the peak activity evoked by 3 μM of Forskolin (FSK). Middle: cAMP GloSensor luciferase activity traces in NOPLight expressing HEK293 cells in response of different concentrations of N/OFQ, normalized to the peak activity evoked by 3 μM of Forskolin (FSK). Right: Quantification of peak cAMP activity of NOPR and NOPLight expressing cells at different concentrations of N/OFQ. (n = 3 independent experiments, data shown as mean ± SEM, two sample t-test, n.s. P = 0.584, *P = 0.0623, **P = 0.00874, ****P < 0.0001). **b**. Representative images of cells co-expressing mCherry-tagged β-arrestin-2 with NOPR (left, scale bar = 20 μm) or NOPLight (right, scale bar = 20 μm) before and 12.5 minutes after N/OFQ (10 μM) stimulation. NOPR and NOPLight are labeled with Alexa-647-conjugated M1 anti-FLAG antibody (M1-647). **c**. Ratio of change in mCherry-tagged β-arrestin-2 signal versus change of M1-647 signal in NOPR and NOPLight expressing cells. (n = 21 and 16 cells respectively, from 3 independent experiments, data shown as mean ± s.d., one-sided Mann-Whitney U test, P<0.0001). **d**. Plasma membrane signal (TIRF) of mCherry-tagged β-arrestin-2 and FLAG-tagged NOPR signal before and after the application of N/OFQ. (n = 3 independent experiments, data shown as mean ± s.e.m) **e.** Similar to **d**, cells expressing NOPLight instead of NOPR. **f.** representative images of NOPLight expressing HEK293T cells at 0 min, 30 min, 60 min, 90 min and 120 min after the addition of N/OFQ (1μM). 5 μM UFP 101 was added at t = 110 min. **g.** Normalized fluorescent response ($\Delta F/F_0$) at time points as in **f.** (n = 3 independent experiments, P = 0.7522 for one-way repeated measures ANOVA test between fluorescence response at 30, 60 and 120 minutes after N/OFQ, P<0.001 for one-way repeated measures ANOVA test between 30, 60, 120 minutes after N/OFQ and after UFP 101.).

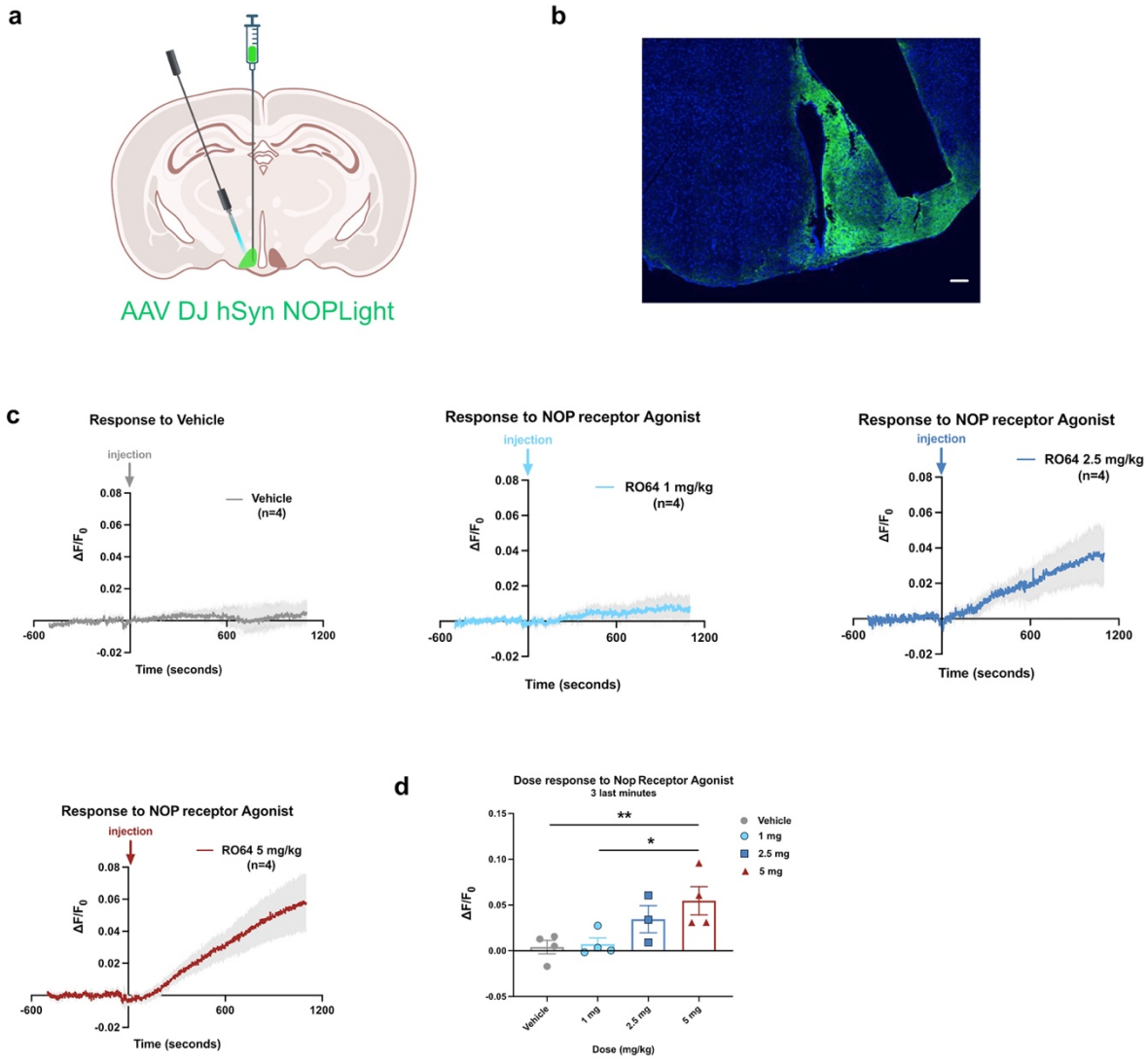
a
AAV DJ hSyn NOPLight
b
c
Response to Vehicle
injection
Vehicle
(n=4)
ΔF/F0
Time (seconds)
Response to NOP receptor Agonist
injection
RO64 1 mg/kg
(n=4)
Response to NOP receptor Agonist
injection
RO64 2.5 mg/kg
(n=4)
Response to NOP receptor Agonist
injection
RO64 5 mg/kg
(n=4)
d
Dose response to Nop Receptor Agonist
3 last minutes
Vehicle
1 mg
2.5 mg
5 mg
Dose (mg/kg)

Supplementary Figure 5. Target engagement of a NOPR agonist in the arcuate nucleus. **a.** Schematic representation showing AAVDJ.hSynapsin1.NOPLight (NOPsyn) (0.8 x 1013 GC/mL) injection into the arcuate nucleus of the hypothalamus (ARC), followed by optic fiber implantation. **b.** Representative image of NOPLight-expressing brain slice showing optic fiber placement. GFP (green) expression, and DAPI in the ARC. Scale bar, 100 µm. **c**. Average in vivo photometry trace ($\Delta F/F_0$) for vehicle response. **d**. Average fluorescence traces showing the response to RO64 injection at 1 mg/kg. **e**. Average fluorescence traces showing the response to RO64 at 2.5 mg/kg. **f**. Average fluorescence traces showing the response to RO64 at 5 mg/kg. All injections were performed I.P. **g**. Quantification of average fluorescence signals in 3-minute bins (957-1137 seconds) at the end of fiber photometry recordings, including data from (**c-f**) vehicle response and the response to RO64 (1, 2.5, and 5 mg/kg) IP injection. n=5 mice. Data are expressed as mean ± standard error of the mean (SEM). One-way ANOVA with Tukey's multiple comparisons test. Vehicle vs. RO64 5 mg/kg **P= 0.0058. RO64 1 mg/kg vs. RO64 5 mg/kg *P= 0.0131.

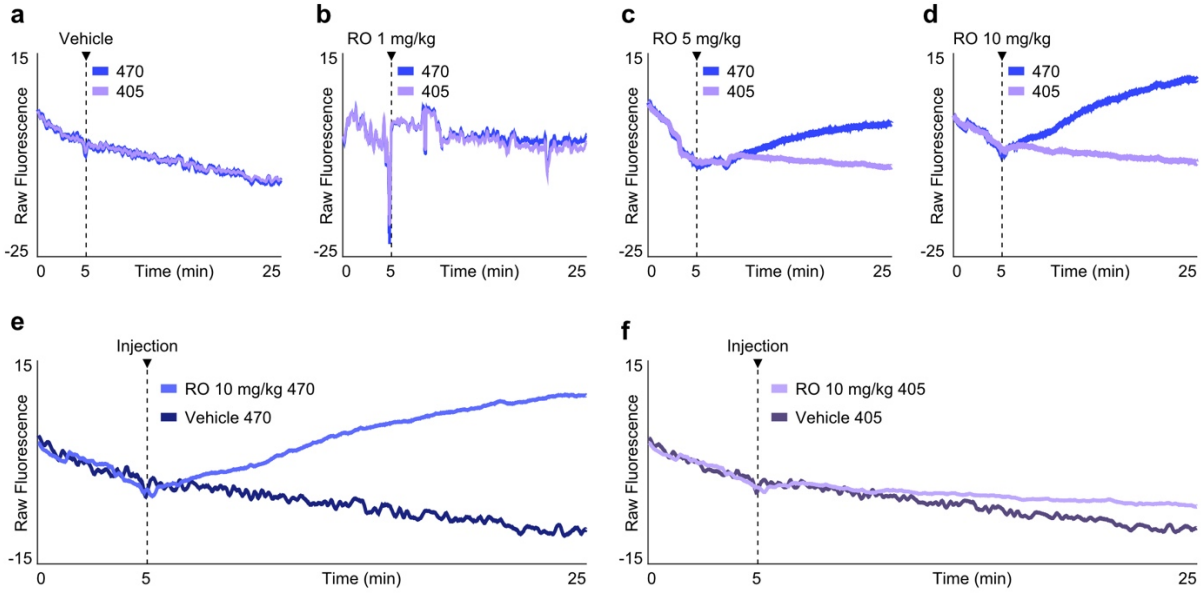
a
Vehicle
470
405
Raw Fluorescence
15
-25
0
5
Time (min)
25
b
RO 1 mg/kg
470
405
Raw Fluorescence
15
-25
0
5
Time (min)
25
c
RO 5 mg/kg
470
405
Raw Fluorescence
15
-25
0
5
Time (min)
25
d
RO 10 mg/kg
470
405
Raw Fluorescence
15
-25
0
5
Time (min)
25
e
Injection
RO 10 mg/kg 470
Vehicle 470
Raw Fluorescence
15
-15
0
5
Time (min)
25
f
Injection
RO 10 mg/kg 405
Vehicle 405
Raw Fluorescence
15
-15
0
5
Time (min)
25

Supplemental Figure 6: 405nm as isosbestic wavelength for NOPLight reports an increase in fluorescence in response to exogenous NOPR agonism.
a-d. Individual 405nm (isosbestic, purple) and 470nm (signal, blue) traces during fiber photometry recordings of NOPLight in response to **a)** vehicle, **b)** 1 mg/kg selective NOPR agonist Ro 64-6198 (RO), **c)** 5 mg/kg RO, or **d)** 10 mg/kg RO for a single, representative animal (M1) from Figure 3c. Initially, the 405nm and 470nm traces both appear to increase in response to the NOPR agonist, suggesting that the 405nm is not an appropriate isosbestic wavelength for NOPLight as it may report ligand-dependent changes in fluorescence. **e.** Unprocessed 470nm traces during NOPLight recording in response to 10 mg/kg RO (light blue) and vehicle (dark blue) for a single, representative animal (M1). **f.** Unprocessed 405nm traces during NOPLight recording in response to 10 mg/kg RO (light purple) and vehicle (dark purple) for a single, representative animal (M1). Both traces have similar decay trends during the baseline period preceding the injection, but after injection the RO 405 trace increases relative to the vehicle trace. This again suggests that the 405nm channel may report changes in NOPLight fluorescence dependent on the presence of a NOPR ligand, indicating that this wavelength is likely not the most appropriate isosbestic point for this sensor.

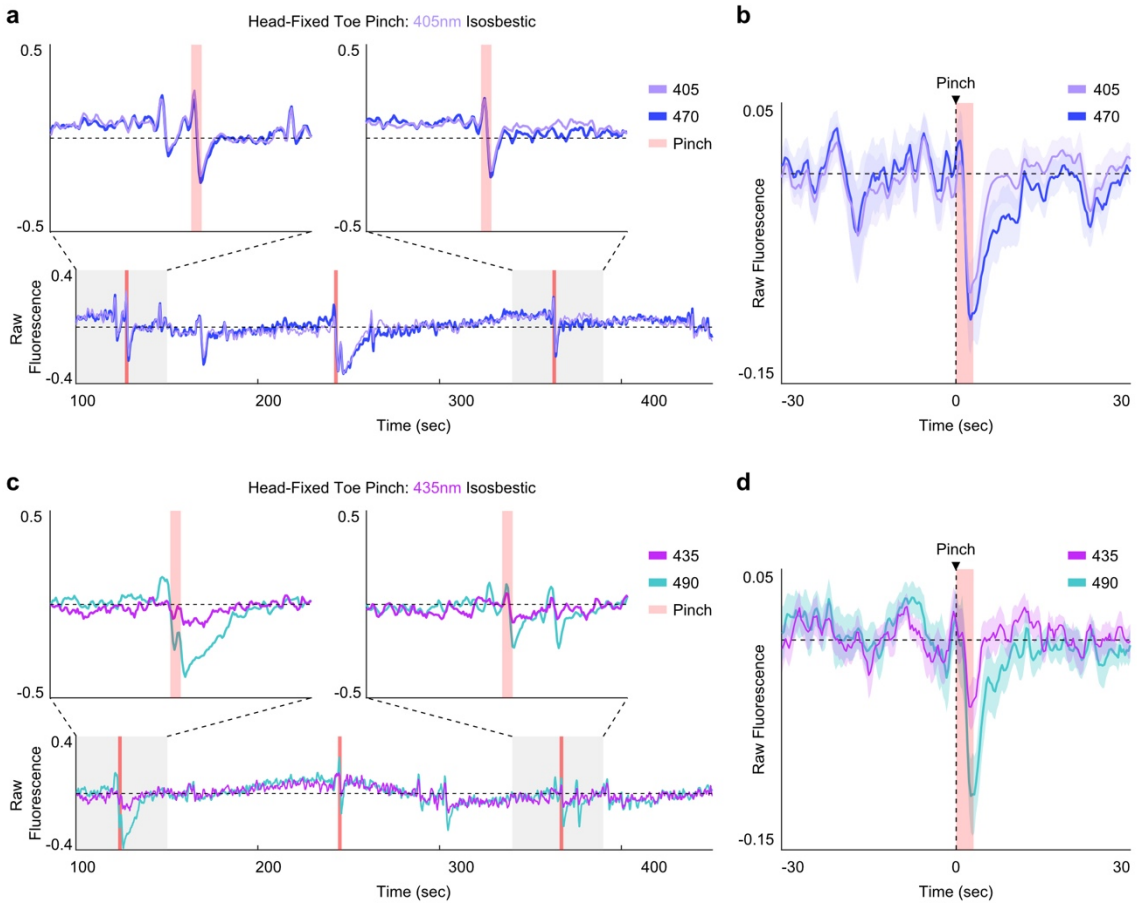
a
Head-Fixed Toe Pinch: 405nm Isosbestic
0.5
-0.5
405
470
Pinch
Raw Fluorescence
0.4
-0.4
100
200
300
400
Time (sec)
b
Pinch
405
470
0.05
-0.15
Raw Fluorescence
-30
0
30
Time (sec)
c
Head-Fixed Toe Pinch: 435nm Isosbestic
0.5
-0.5
435
490
Pinch
Raw Fluorescence
0.4
-0.4
100
200
300
400
Time (sec)
d
Pinch
435
490
0.05
-0.15
Raw Fluorescence
-30
0
30
Time (sec)

Supplemental Figure 7: NOPLight detection of stress-induced endogenous N/OFQ release using two different sets of isosbestic and signal wavelengths.
a. Representative 405nm (isosbestic, purple) and 470nm (signal, blue) traces for a single, head-fixed fiber photometry recording (M3) of NOPLight fluorescence following repeated exposure to a brief, acute stressor (toe pinch).The 405nm trace closely follows the 470nm trace throughout the entire recording. In combination with minimization of motion artifact due to head-fixation, this suggests that the 405nm trace is reporting ligand-bound dependent changes in NOPLight fluorescence. **b.** Averaged 405nm (isosbestic, purple) and 470nm (signal, blue) raw fluorescence traces across all animals and all events. The 405nm trace closely follows the 470nm trace during the entire pinch event period. Data represented as mean ± SEM **c.** Representative 435nm (isosbestic, purple) and 490nm (signal, blue) traces for a single, head-fixed fiber photometry recording (M3) of NOPLight fluorescence following repeated exposure to a brief, acute stressor (toe pinch).The 435nm trace fluctuates independently from the 470nm trace throughout the recording. **d.** Averaged 435nm (isosbestic, purple) and 490nm (signal, blue) raw fluorescence traces across all animals and all events. The 435nm trace does report an overall similar trend to the 490nm during the pinch event period, but on a smaller scale such that the decrease in NOPLight signal reflected in the 490nm trace alone is still detectable following subtraction of the 435nm isosbestic trace. Together, the results show NOPLight detection of naturalistic endogenous N/OFQ release during a stressful event. They also suggest that 435nm is a more appropriate isosbestic point for NOPLight than 405nm. Data represented as mean ± SEM

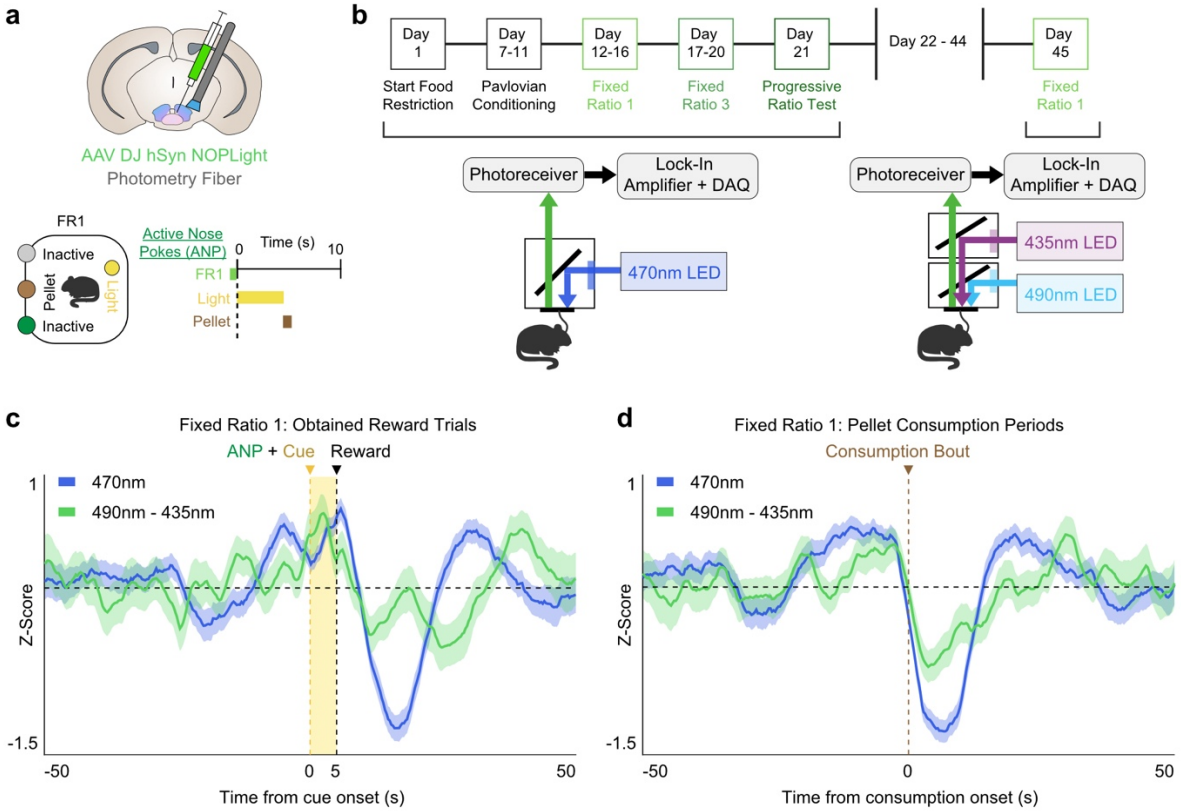
a
AAV DJ hSyn NOPLight
Photometry Fiber
FR1
Inactive
Pellet
Light
Inactive
Active Nose Pokes (ANP)
Time (s)
0
10
FR1
Light
Pellet
b
Day 1
Start Food Restriction
Day 7-11
Pavlovian Conditioning
Day 12-16
Fixed Ratio 1
Day 17-20
Fixed Ratio 3
Day 21
Progressive Ratio Test
Day 22 - 44
Day 45
Fixed Ratio 1
Photoreceiver
Lock-In Amplifier + DAQ
470nm LED
Photoreceiver
Lock-In Amplifier + DAQ
435nm LED
490nm LED
c
Fixed Ratio 1: Obtained Reward Trials
ANP + Cue
Reward
470nm
490nm - 435nm
Z-Score
1
-1.5
-50
0
5
50
Time from cue onset (s)
d
Fixed Ratio 1: Pellet Consumption Periods
Consumption Bout
470nm
490nm - 435nm
Z-Score
1
-1.5
-50
0
50
Time from consumption onset (s)

Supplemental Figure 8: Evaluation of two isosbestic wavelengths for NOPLight during reward-related operant conditioning.
a. Top: Coronal brain cartoon of viral injection of NOPLight and fiber implant in the VTA of WT mice (n = 3). Bottom: Cartoon depicting operant box setup and trial structure for a fixed ratio 1 (FR1) training session. **b.** Timeline depicting training regimen for Pavlovian conditioning and operant conditioning with fiber photometry recording using a 470nm LED excitation wavelength. 24 days after testing, mice were re-tested in a single FR1 session and recorded using 435nm and 490nm LEDs. **c.** Trace of mean NOPLight signal during the FR1 reward period for the 470nm signal (blue) or the 490nm – 435nm signal (green), aligned to reinforced active nosepokes. Only trials where the animal retrieved the reward within 50s of its delivery are included. Both traces show similar overall trends in activity during the event window (peak during cue, decrease following reward delivery). Data represented as mean ± SEM **d.** Trace of mean NOPLight signal aligned to reward consumption during an FR1 session for the 470nm signal (blue) or the 490nm – 435nm signal (green). Both traces show similar trends during the reward consumption period (decrease during consumption, increase upon termination of a consumption bout). Data represented as mean ± SEM